Department of Physics and Astronomy
Heidelberg University

An Optical Dipole Trap with Tunable Geometry for Dysprosium

Bachelor Thesis in Physics
submitted by

Paul Holzenkamp
born in Mannheim

on the

22.09.2022

Supervisor and first examiner: Prof. Dr. Lauriane Chomaz
Second examiner: Prof. Dr. Wolfram Pernice

Abstract

In this thesis first the theoretical basis for optical trapping is presented. After that a calculation regarding the modulation of a Gaussian beam potential by means of an acousto-optical deflector (AOD) is done to describe the generated time averaged potentials. A time averaged potential with a shape similar to a Gaussian beam potential is characterised with regards to its depth and width as well as compared to the Gaussian beam potential. Once the theoretical predictions are made a set-up to produce such a modulated potential is presented and tested. The modulated potentials that were compared to calculated predictions used the modulation functions sine, ramp/linear, square-wave and arccosine of which the last one produces the potential close to a Gaussian beam potential. The set-up was found to be able to produce time averaged potentials with an aspect ratio of up to ca. 6.

Zusammenfassung

In dieser Arbeit werden zunächst die theoretischen Grundlagen für optische Fallen vorgestellt. Anschließend wird eine Berechnung zur Modulation eines Gaußstrahlpotentials mittels eines akusto-optischen Deflektors (AOD) durchgeführt, welche die erzeugten zeitgemittelten Potentiale zu beschreibt. Ein zeitgemitteltes Potential mit einer dem Gaußstrahlpotential ähnlichen Form wird hinsichtlich seiner Tiefe und Breite charakterisiert und mit dem Gaußstrahlpotential verglichen. Nachdem die theoretischen Vorhersagen gemacht wurden, wird ein Aufbau zur Erzeugung eines solchen modulierten Potentials vorgestellt und getestet. Für die modulierten Potentiale, die mit den berechneten Vorhersagen verglichen wurden, wurden die Modulationsfunktionen Sinus, Lineare bzw. Dreiecksfunktion, Rechtecksfunktion und Arkuskosinus verwendet, von denen die letzte ein Potential erzeugt, das einem Gaußstrahlpotential nahe kommt. Es wurde festgestellt, dass der Aufbau in der Lage ist, zeitlich gemittelte Potentiale mit einem Aspektverhältnis von bis zu ca. 6 zu erzeugen.

Contents

1 Introduction

1.1 Motivation and Context

The experiment in the course of which this thesis was written has the goal to study quantum gases of Dysprosium at ultra-low temperatures. The ultra-low temperatures give rise to different interesting phenomena with one of them being the possibility to prepare the vast majority of atoms in their ground state. Due to the greatly reduced movement and thus low energy of the atoms this provides the opportunity of great control over the atoms as they are unlikely to receive enough energy to change their state. This allows to prepare a spin-polarised gas in which all or at least the vast majority of atoms have the magnetic sublevel $M_J = -J$ of the total angular momentum J which makes it possible to investigate the long-range magnetic dipole interaction of Dysprosium atoms. As this long-range interaction results from the magnetic moment of the atoms Dysprosium is the most suitable element for this kind of experiment as its ground-state has the largest magnetic moment out of all the elements of the periodic table.
The interaction of Dysprosium atoms consists of two interaction types, one being the aforementioned magnetic dipole interaction, which is long-range and anisotropic, and the second one being the short-range, isotropic contact interaction. This is interesting because the strength of the contact interaction can be tuned by an external magnetic field when close to a Feshbach resonance such that one can observe the interaction of Dysprosium atoms for different relative strengths of the long-range and short-range interactions [Chi+10] [GGP02].
For this tuning to be accessible one needs to confine the quantum gases without using any magnetic fields which leads to optical dipole traps (ODTs) as they produce a trapping potential for neutral atoms solely relying on the light-matter interaction of the laser light with the atoms. In the case of far-detuned ODTs like in this experiment one suppresses the driving of transitions of the atoms to reduce photon scattering and thus the probability of heating and losing atoms [GWO99].

In the experiment of the Quantum Fluids group the atoms will be precooled in a 2D- and 3D-MOT before they will be transferred to the ODT. For more information on this set-up before the ODT refer to the Bachelor thesis by Christian Gölzhäuser from 2021 [Göl21] or the Master thesis by Joschka Schöner from 2022 [Sch22].

The tunable geometry that is the topic of this thesis has two possible purposes: The first would be the opportunity to use different shapes of potentials without the need for additional optical set-ups and the second but more fundamental reason to use a tunable geometry is the loading of the trap. When loading the ODT from the 3D-MOT the goal is to maximise the amount of atoms that are kept trapped. To achieve this one should have a good overlap of the volumes of the MOT and the ODT [ATS05]. As the ODT finally will be used to have very cold and dense gas cloud as necessary to reach degeneracy, i.e. a BEC, its volume should not be very large. This results in a conflict with the condition of a large volume overlap with the bigger MOT when loading which can be resolved with a tunable geometry as the size of the trap can be large for loading and then be reduced while cooling.
The specifics of the implementation of an ODT in the actual experiment of the group will not be covered here as this is a preparatory work. The experiment is not yet at the point where the ODT is needed.

1.2 Properties of Dysprosium

Another reason why Dysprosium ($_{66}$Dy) is an interesting element for an experiment is due to the abundance in different stable isotopes (see table 1). Two of the five isotopes listed in table 1 are fermionic and three are bosonic which further allows to investigate systems of both statistics from the same element.

isotope	^{160}Dy	^{161}Dy	^{162}Dy	^{163}Dy	^{164}Dy
mass [u]	159.925	160.927	161.927	162.929	163.929
abundance [%]	2.3	18.9	25.5	24.9	28.3

Table 1: *Weights and abundances of the 5 most common Dysprosium isotopes from [Lae+03, p.777]. The unit u is the unified atomic mass unit [Poi19, p.146]. The average weight of Dysprosium is given as* 162.5 u.

Another important property of Dysprosium is the total angular momentum J as well as the resulting magnetic moment μ_m. The total angular momentum of the ground-state is independent of the isotope given as $J = 8$. The magnetic moment of the ground-state with $M_J = -J$ of Dysprosium is roughly $\mu_m \approx -10\mu_B$ and for the fermionic isotopes it depends on the hyperfine structure [see Mai15, pp.21-22].

Further one needs to know the polarisability of Dysprosium for the optical dipole trap. For this the wavelength of the laser is important which in this experiment is given by $\lambda = 1064\,\text{nm}$. At this wavelength the relevant polarisabilities, given in units of $4\pi\epsilon_0 a_0^3$ (atomic units, ϵ_0 is the vacuum permittivity and a_0 the Bohr radius), are experimentally found to be $\Re(\alpha_s) = 184.4 \pm 2.4$ and $\Re(\alpha_t) = 1.7 \pm 0.6$ [Rav+18] and theoretically were determined to $\Re(\alpha_s) = 193$ and $\Re(\alpha_t) = 1.3$ [Li+16]. The polarisability will be introduced in section 2.1.

2 Theory of Optical Trapping

This chapter explains how light forms a potential for atoms first in the general case and then for the specific situation of the experiment this thesis is based on. That means after the general introduction the potential for the case of Dysprosium atoms in linearly polarised light will be shown for a single Gaussian beam as well as two crossed Gaussian beams.

2.1 Optical trapping potential, polarisability and the case of dysprosium atoms

Consider an atom in an electric field $\mathbf{E}$. The electric field induces an atomic dipole moment $\mathbf{p}$ which is proportional to the electric field. The so called polarisability α then determines, like the name suggests, how strongly the atom is polarised:

$$\mathbf{p} = \alpha \mathbf{E} \tag{1}$$

For a general oscillating electric field $\mathbf{E}(\mathbf{r}, t) = \hat{\mathbf{e}} E(\mathbf{r}) \exp(i(\omega t - \mathbf{kr})) + const.$, e.g. one produced by a laser with unit polarisation vector $\hat{\mathbf{e}}$, amplitude E, angular frequency ω and wavevector $\mathbf{k} = \frac{2\pi}{\lambda}\hat{\mathbf{k}} = \frac{\omega}{c}\hat{\mathbf{k}}$, the polarisability is a complex-valued tensor which is depended on the angular frequency ω of the oscillation [see Ilz20, p.24]. The resulting potential for atoms in the electric field is then given by [GWO99, p.3]

$$U = -\frac{1}{2} \langle \mathbf{pE} \rangle \tag{2}$$

with $\langle \cdot \rangle$ denoting a time-average and the $\frac{1}{2}$ stemming from the fact that $\mathbf{p}$ is an induced dipole. With the intensity

$$I = 2\epsilon_0 c \left|\mathbf{E}\right|^2 \tag{3}$$

ϵ_0 being the vacuum permittivity and c being the speed of light, one gets the general potential at position $\mathbf{r}$ of atoms in the electric field and an homogeneous magnetic field [LWD14, p.2]

$$\begin{aligned} U(\mathbf{r}; \theta_k, \theta_p, \mathcal{A}, \omega) = -\frac{1}{2\epsilon_0 c} I(\mathbf{r}) \cdot \\ \Big[\Re(\alpha_\mathrm{s}(\omega)) + \\ \mathcal{A} \cos(\theta_k) \frac{M_J}{2J} \Re(\alpha_\mathrm{v}(\omega)) + \\ \frac{3M_J^2 - J(J+1)}{J(2J-1)} \cdot \frac{3\cos^2(\theta_p) - 1}{2} \Re(\alpha_\mathrm{t}(\omega)) \Big] \end{aligned} \tag{4}$$

$\alpha_\mathrm{s}, \alpha_\mathrm{v}, \alpha_\mathrm{t}$ are the scalar, vector and tensor parts of α. Information regarding the theoretical evaluation of these can be found in the literature [LWD14] and [Li+16]. The former only shows the formula whereas the latter also calculates the values. J is the total angular momentum quantum number and M_J is the corresponding quantum number defining the magnetic sublevel of the state of the atom. θ_k is the angle between the quantisation axis of M_J, given by the external magnetic field, and the wave vector $\mathbf{k}$ of the electric field. θ_p is in turn the angle between said quantisation axis and the polarisation vector and $\mathcal{A}$ expresses the polarisation of the light with $\mathcal{A} = \pm 1$ being circular polarisation (+ : right, - : left) light

and $\mathcal{A} = 0$ being linear polarisation.
For simplicity the term in brackets in (4) will be noted as the scaling factor $\tilde{\alpha}$:

$$U(\mathbf{r}; \theta_k, \theta_p, \mathcal{A}, \omega) = -\frac{\tilde{\alpha}(\omega, \theta_k, \theta_p, \mathcal{A})}{2\epsilon_0 c} I(\mathbf{r}) \tag{5}$$

This $\tilde{\alpha}$ will in fact turn out to be (almost) constant for the intended experiment set-up. Said set-up is a far red-detuned laser with wavelength $\lambda = 1064\,\text{nm}$ and arbitrarily oriented linear polarised light. This set-up will fix $\omega = 2\pi\frac{c}{\lambda}$ via the laser wavelength, $\mathcal{A} = 0$ due to the linear polarisation of the laser and also θ_p to the arbitrary angle between the magnetic field and the laser polarisation. Therefore the relevant values, given in units of $4\pi\epsilon_0 a_0^3$ (atomic units), are $\Re(\alpha_s) = 184.4 \pm 2.4$ and $\Re(\alpha_t) = 1.7 \pm 0.6$ for the given wavelength as found by [Rav+18] [1]. This experimental result is a rather new one that also determined the tensor polarisability and matches quite well with the theory [Li+16] where $\Re(\alpha_s) = 193$ and $\Re(\alpha_t) = 1.3$.
As the vector part drops out and the tensor part is two orders of magnitude smaller than the scalar polarisability the polarisability can be approximated to be constant. Thus to put it in a simple form the formula relating the potential created by light to its intensity is given with the positive constant $\mathfrak{c} = \frac{\tilde{\alpha}}{2\epsilon_0 c} > 0$ and all dependencies other than the position will be disregarded as they are fixed or not important in our case:

$$U(\mathbf{r}) = -\mathfrak{c} I(\mathbf{r}) \tag{6}$$

For more in-depth information regarding the influence of the tensor polarisability refer to the Appendix A.3.

2.2 Optical trapping potential of a single Gaussian beam

As we now have a general understanding of how a general intensity distribution of light will introduce a potential for our case we will now specify the used laser beam to be Gaussian. All we have to do for this is to combine the intensity distribution of a Gaussian beam (see A.1) and (6):

$$U(x, y, z) = -\frac{2P\mathfrak{c}}{\pi w_x(y) w_z(y)} \exp\left(-2\left(\frac{x^2}{w_x^2(y)} + \frac{z^2}{w_z^2(y)}\right)\right) \tag{7}$$

$$\hat{U} = |\min U| = |U(0,0,0)| = \frac{2P\mathfrak{c}}{\pi w_x w_z} \tag{8}$$

with

$$w_i(y) = w_i\sqrt{1 + \frac{y^2}{z_{R,i}^2}}; \qquad z_{R,i} = \frac{\pi w_i^2}{\lambda} \tag{9}$$

$\hat{U}$ is the trap depth, which is often given in units of temperature by dividing it by Boltzmann's constant k_B as a characteristic of a trap. This also applies in general for depictions of any potential.

This is a conserving potential and the resulting force is pointing towards the beam focus at $\mathbf{r} = (0, 0, 0)$. This is easy to see as the potential is proportional to the intensity of the

[1] There are also other works that determine the polarisability of dysprosium experimentally, although they do not give a tensor polarisability. Examples are [Lu14] with $\Re(\alpha) \approx 75$ or [Wen15] with $\Re(\alpha) = 82 \pm 13$

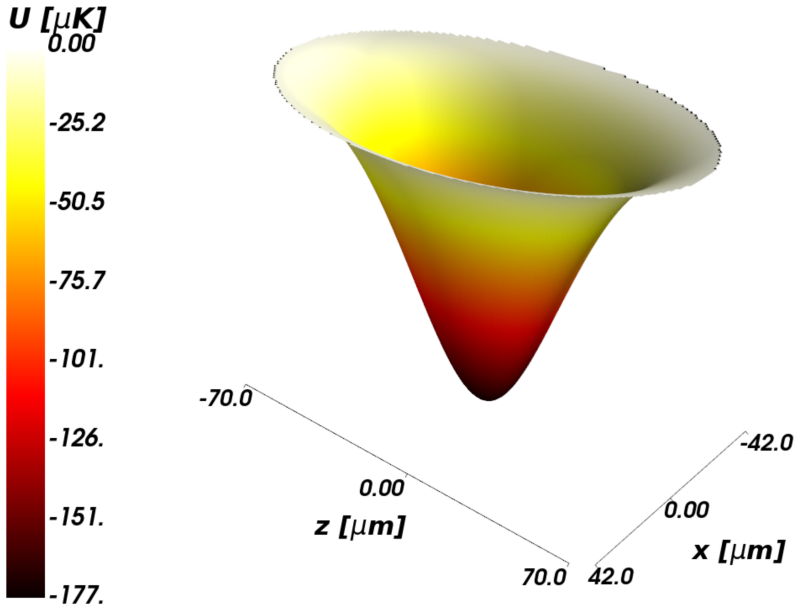

Figure 1: *Plot of a Gaussian beam potential for waists* $w_x = 30\,\mu$m, $w_z = 50\,\mu$m *and power* $P = 10\,$W *at the focus* ($y = 0$).

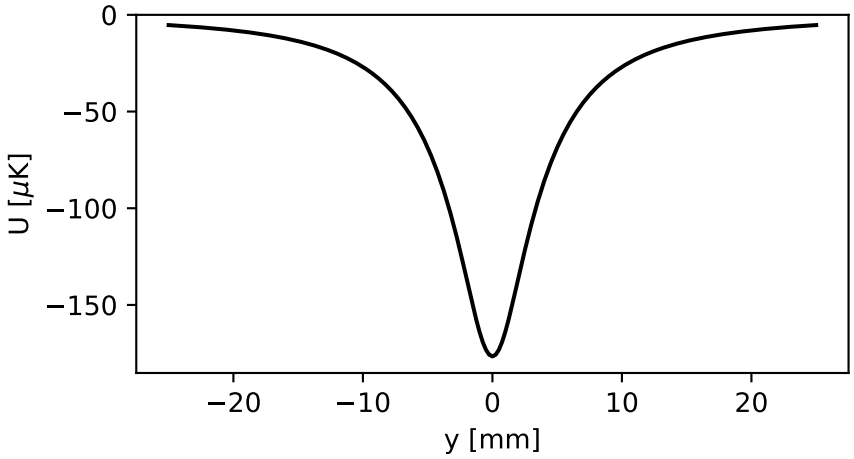

Figure 2: *Plot of a Gaussian beam potential for waists* $w_x = 30\,\mu$m, $w_z = 50\,\mu$m *and power* $P = 10\,$W *along the propagation direction* y ($x = z = 0$).

laser beam which is highest at the focus and monotonically decreases away from it. For the directions perpendicular to the propagation direction this can be seen in figure 1. Here the potential created by an elliptical Gaussian beam is shown at the focus of said beam. One can nicely see that the ratio of the beam waists in x- and z-direction of $\frac{3}{5}$ is also present in the shape of the potential.
The potential along the propagation axis is shown in figure 2. One can also see here that the potential has a clear minimum at the focus. Further the potential seen here corresponds to the minimum of figure 1 at different positions for y, which nicely illustrates that the trap gets shallower further away from the focus. An effect that is not as apparent from the plots but also relevant is that the potential shown in figure 1 doesn't only get shallower but also wider, which is necessary to still retain the same amount of cumulative intensity and thus energy in every slice along the propagation direction. Both of these effects are clear also from the definition of the potential in (7).
Further one has to notice that the confinement of the optical potential in propagation direction is very weak compared to the other two directions as the length scales here are, in this example, more than two orders of magnitude apart.

2.2.1 Harmonic Approximation

An often used approximation for the region close to the potential minimum, which requires the thermal energy of the atoms to be much smaller than the trap depth ($k_B T \ll \left|\hat{U}\right|$), is the harmonic approximation. It allows to get a very simple model for the movement of the atoms close to the center of the trap and the typical timescales involved. The harmonic approximation is the Taylor expansion to the 2$^{\text{nd}}$ order:

$$U \approx -\hat{U} + \nabla U|_{(0,0,0)} \cdot \begin{pmatrix} x \\ y \\ z \end{pmatrix} + \frac{1}{2} \left(x, y, z\right) \cdot \left(\mathrm{H}U|_{(0,0,0)}\right) \cdot \begin{pmatrix} x \\ y \\ z \end{pmatrix} \tag{10}$$

Here HU denotes the Hesse-matrix. This results in the following form:

$$U \approx -\hat{U} \left(1 - \frac{2x^2}{w_x^2} - \frac{2z^2}{w_z^2} - \frac{y^2}{2z_{R_{\text{eff}}}^2}\right) \tag{11}$$

with

$$\frac{1}{z_{R_{\text{eff}}}^2} = \left(\frac{1}{z_{R_x}^2} + \frac{1}{z_{R_z}^2}\right) \Leftrightarrow z_{R_{\text{eff}}} = \frac{z_{R_x} z_{R_z}}{\sqrt{z_{R_x}^2 + z_{R_z}^2}} \tag{12}$$

or expressed via the beam waists:

$$z_{R_{\text{eff}}} = \frac{\pi}{\lambda} \cdot \frac{w_x^2 w_z^2}{\sqrt{w_x^4 + w_z^4}} \tag{13}$$

(11) can be described by the more common form

$$U \approx -\hat{U} + \frac{1}{2} m\omega_x^2 x^2 + \frac{1}{2} m\omega_z^2 z^2 + \frac{1}{2} m\omega_y^2 y^2 \tag{14}$$

with the so called trapping frequencies

$$\omega_{x,z} = \sqrt{\frac{4\hat{U}}{m w_{x,z}^2}} \qquad \omega_y = \sqrt{\frac{\hat{U}}{m z_{R_{\text{eff}}}^2}} \tag{15}$$

Using for example the parameters from figure 1 one gets the values $\omega_x = 2\pi \cdot 1009\,\text{Hz}$, $\omega_z = 2\pi \cdot 605\,\text{Hz}$ and $\omega_y = 2\pi \cdot 6\,\text{Hz}$. This then clearly shows that the atoms are more strongly confined perpendicular to the propagation direction than along it in the conditions that usually apply in the experiment.

2.3 Optical trapping potential of crossed Gaussian beams

As seen in the section above a weakly focused single Gaussian beam usually provides unsatisfying confinement in the propagation direction. To counteract this one uses two crossed Gaussian beams, that intersect at their respective foci and whose propagation directions are not parallel and will be assumed to be 90° in the following. The idea is that the weak confinement along the propagation direction of one beam is compensated for by the other beam as for this beam that direction is perpendicular to its propagation direction.

In the case of crossed beams one has to simply add the corresponding single beam potentials, given that it is ensured that there is no significant interference. In the case of an angle of 90° between the two beams (one beam propagates along the y-axis and the other one along the x-axis) one therefore gets:

$$U = -\hat{U}_1 \frac{\exp\left(-2\left(\frac{x^2}{w_{x,1}^2(y)} - \frac{z^2}{w_{z,1}^2(y)}\right)\right)}{\sqrt{1+\frac{y^2}{z_{R,x,1}^2}}\sqrt{1+\frac{y^2}{z_{R,z,1}^2}}} + \hat{U}_2 \frac{\exp\left(-2\left(\frac{y^2}{w_{y,2}^2(x)} + \frac{z^2}{w_{z,2}^2(x)}\right)\right)}{\sqrt{1+\frac{x^2}{z_{R,y,2}^2}}\sqrt{1+\frac{x^2}{z_{R,z,2}^2}}} \tag{16}$$

$$\approx -\hat{U}_1 - \hat{U}_2 + \frac{m}{2}\left(\tilde{\omega}_x^2 x^2 + \tilde{\omega}_y^2 y^2 + \tilde{\omega}_z^2 z^2\right) \quad \text{with } \tilde{\omega}_i = \sqrt{\omega_{i,1}^2 + \omega_{i,2}^2} \tag{17}$$

For the interested reader: If the beams do not have an angle of exactly 90° between them one has to calculate $\tilde{\omega}$ a bit differently [Bai12, pp. 21-28].

3 Optical potential and laser beam modulation

Modulating a laser beam of the trap allows to modulate the trapping potential. This is especially of interest in the loading phase and the evaporative cooling phase for an optical dipole trap (ODT). In the former case, the reason is the ability to adjust to the volume of the 3-dimensional-magneto-optical-trap (3D-MOT) when loading which allows to increase loading efficiency as it is proportional to the overlap volume of ODT and 3D-MOT [ATS05]. In the evaporative cooling phase, where one lowers the trap depth to lose atoms with high energy, the control over the trap geometry also allows to keep the trap as tight as wanted. This can be important as lowering the power in the trap reduces the trapping frequencies (see (15)) which makes the confinement provided by the trap weaker, i.e. it allows the atom cloud to expand.

There are different ways to achieve control over the trap geometry and here the chosen method is a time averaged potential by means of an acousto-optic deflector (AOD). Another method which works for large optical power would be the use of cylindrical lenses to actually change the shape of the beam. This has the benefit that one does not have to time average the potential to get the wanted shape and thus knows exactly what shape the beam has as it is still Gaussian. A disadvantage of this set-up is the need for a fast and precise translation stage [Pol17], which is subject to wear. Also one is more limited in the trap shape that can be achieved, as the cylindrical lenses are planned for one potential shape (Gaussian), whereas with an AOD different modulation functions produce different potential shapes.

With an AOD the modulation of the potential shape happens by moving the beam following a periodic pattern. Without further restrictions on the modulation this periodic movement could just result in the trapping potential being moved with the atoms following. Hence it would result in heating of the atom cloud which is clearly undesirable.
To avoid this one has to do this modulation of the beam on a timescale far shorter than the timescales of the trap, which are given by the trapping frequencies (15). Therefore the modulation frequency has to be far greater than the trapping frequencies. Assuming a single round Gaussian beam with waist $w = 30\,\mu\text{m}$, laser power $P = 10\,\text{W}$ and Dysprosium atoms with mass $m = 162.5\,\text{u}$ (u being the unified atomic mass unit [Poi19, p.146]) the radial trapping frequency is $\omega \approx 2\pi \cdot 1302\,\text{Hz}$ and thus the modulation frequency has to be significantly larger. One could also use higher power for larger trapping frequencies, e.g. $P = 40W$ would double the trapping frequencies, thus one needs $f_{\text{mod}} \gg$ few kHz. One would like the modulation frequency to by at least an order of magnitude larger than the trapping frequencies. As there are limitations given by the circuit generating the radio-frequency-signal (RF-signal) to how fast one can modulate, one also has an upper limit for the modulation frequency (see 4.1). Therefore one should choose a modulation frequency around 20 kHz to 30 kHz. In this case the atoms only experience the time averaged potential generated by periodically moving the beam around. One can then shape this time averaged potential via choice of the modulation function (e.g. an arccosine or a linear function) and choice of the modulation amplitude.
As the beam is the same beam as before being moved and now is just moved in position over time, none of the beam characteristics actually change. This has to be kept in mind when working with an AOD here because this determines how the beam behaves at lenses.

Only one out of two beams for the crossed ODT will be modulated via an AOD in this experiment, which is why in the following only one single Gaussian beam will be considered.

3.1 Time averaged potential - Calculation

A time averaged potential is as the name suggests the time average, denoted by $\langle\cdot\rangle$, over a given time-dependent potential U that will here be assumed to be periodic in time with period T.

$$\langle U\rangle = \frac{1}{T}\int_0^T U\mathrm{d}t \tag{18}$$

In this case the potential generated by a single Gaussian beam (7), where the position of the beam in x-direction is modulated by some periodic function $x_{\mathrm{mod}}(t)$ with period T, will be used:

$$U_{\mathrm{mod}}(x,y,z) = \langle U(x - x_{\mathrm{mod}}(t), y, z)\rangle \tag{19}$$

$$= \frac{-2P\mathfrak{c}}{\pi w_x(y) w_z(y)} \exp\left(-2\frac{z^2}{w_z^2(y)}\right) \frac{1}{T}\int_0^T \exp\left(-2\frac{(x - x_{\mathrm{mod}}(t))^2}{w_x^2(y)}\right)\mathrm{d}t \tag{20}$$

If the modulation function takes the form $x_{\mathrm{mod}}(t) = \hat{x}\xi(t)$ with an amplitude $\hat{x}$ and $\xi(t) \in [-1,1]\ \forall t \in [0,T]$ all distances in the integral can easily be expressed relative to the modulation amplitude. Therefore one can see that the result of the integral only depends on the dimensionless quantities $q(y) = \frac{w_x(y)}{\hat{x}}$, $\tilde{x} = \frac{x}{\hat{x}}$ as well as the normalised modulation function $\xi(t)$:

$$\frac{1}{T}\int_0^T \exp\left(-2\frac{(x - x_{\mathrm{mod}}(t))^2}{w_x^2(y)}\right)\mathrm{d}t = \frac{1}{T}\int_0^T \exp\left(-2\frac{(\tilde{x} - \xi(t))^2}{q^2(y)}\right)\mathrm{d}t \tag{21}$$

$$= -\frac{1}{T}\int_{\mu(0)}^{\mu(T)} \exp\left(-2\frac{\mu^2}{q^2(y)}\right)\frac{\mathrm{d}\mu}{\xi'\left(\xi^{-1}(\tilde{x} - \mu)\right)} \tag{22}$$

Via substitution one gets the second equality under the assumption that the modulation function is invertible and differentiable:

$$\mu = \tilde{x} - \xi(t) \Leftrightarrow t = \xi^{-1}(\tilde{x} - \mu) \tag{23}$$

$$\Rightarrow \frac{\mathrm{d}\mu}{\mathrm{d}t} = -\xi'(t) \tag{24}$$

$$\Rightarrow \mathrm{d}t = -\frac{\mathrm{d}\mu}{\xi'\left(\xi^{-1}(\tilde{x} - \mu)\right)} \tag{25}$$

3.1.1 Calculation with arccosine-modulation

In the following the calculation for a modulation with an arccosine will be shown as an example[2]. The arccosine was chosen because it produces a time averaged potential with a shape close to the potential of an unmodulated Gaussian beam.
For a modulation with an arccosine in the form described above one gets for $\xi(t)$:

$$\xi(t) = \frac{2}{\pi}\arccos\left(\frac{2t}{T} - 1\right) - 1, \quad t \in [0,T] \tag{26}$$

[2]For other modulation functions see Appendix B

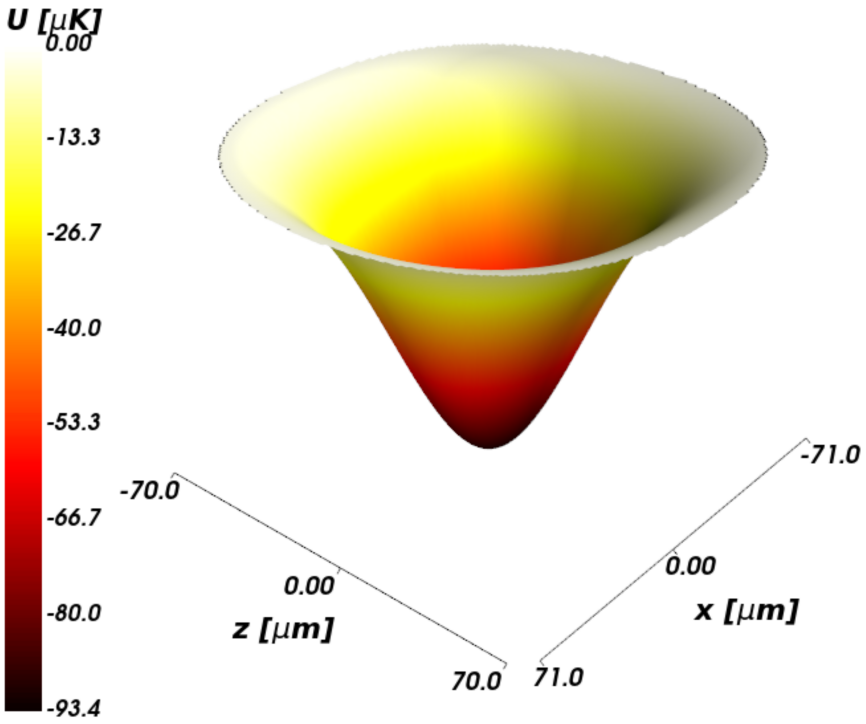

Figure 3: *Plot of a modulated Gaussian beam potential for waists* $w_x = 30\,\mu$m, $w_z = 50\,\mu$m, *power* $P = 10\,$W *and modulation with an arccosine (26) with modulation amplitude* $x_{mod} = 50\,\mu$m *at the focus* ($y = 0$).

Hence one gets

$$\xi'(t) = \frac{4}{T\pi}\frac{1}{\sqrt{1-\left(\frac{2t}{T}-1\right)^2}} \tag{27}$$

$$\xi^{-1}(\zeta) = \frac{T}{2}\left[\cos\left(\frac{\pi}{2}(\zeta+1)\right)+1\right] \tag{28}$$

$$\Rightarrow \xi'(\xi^{-1}(\zeta)) = \frac{4}{T\pi}\frac{1}{\sin\left(\frac{\pi}{2}(\zeta+1)\right)} = \frac{4}{T\pi}\frac{1}{\cos\left(\frac{\pi}{2}\zeta\right)} \tag{29}$$

$$\Rightarrow \frac{1}{\xi'(\xi^{-1}(\tilde{x}-\mu))} = T\frac{\pi}{4}\cos\left(\frac{\pi}{2}(\tilde{x}-\mu)\right) \tag{30}$$

The resulting potential is thus given by

$$U_{\text{mod}}(x,y,z) = \frac{P\mathfrak{c}}{2w_x(y)w_z(y)}\exp\left(-2\frac{z^2}{w_z^2(y)}\right)\cdot\int_{\tilde{x}-1}^{\tilde{x}+1}\cos\left(\frac{\pi}{2}(\tilde{x}-\mu)\right)\exp\left(-2\frac{\mu^2}{q^2(y)}\right)\mathrm{d}\mu \tag{31}$$

In this case the integral does not have an analytical solution so one needs to rely on numerical integration. The benefit of writing it in this form is that only the parameters $\tilde{x}$ and $q(y)$ remain whereas the period drops out.

In figure 3 the potential generated by time averaging the Gaussian beam from figure 1 modulated with an arccosine in the x-direction with a modulation amplitude of 50 µm is shown.

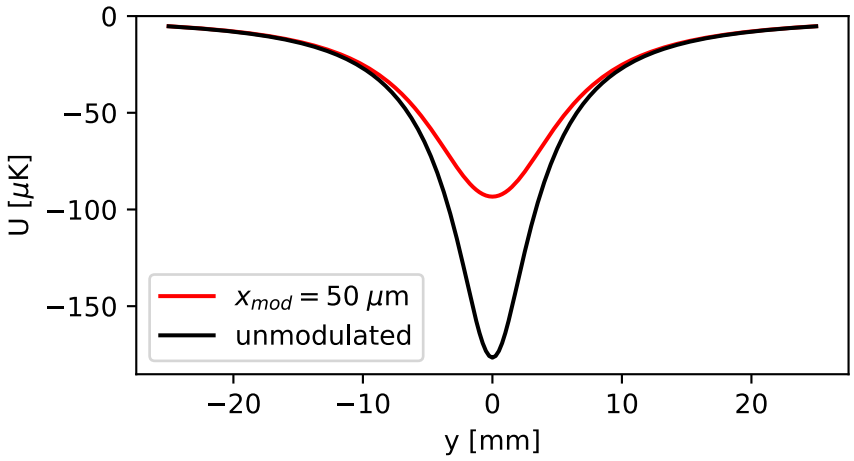

Figure 4: *Plot of a modulated Gaussian beam potential and the corresponding unmodulated potential for waists* $w_x = 30\,\mu m$, $w_z = 50\,\mu m$, *power* $P = 10\,W$ *and modulation with an arccosine (26) with modulation amplitude* $x_{mod} = 50\,\mu m$ *along the propagation direction* y *(*$x = z = 0$*).*

This leads here to a potential which is slightly more elongated in the x-direction than the z-direction in contrast to the unmodulated potential. Another difference to the unmodulated potential is that the trap is shallower than before, due to the fact that the power of the beam as a whole stayed the same and is now spread over a larger area.
As will later be discussed (see 5.2) the goal will be to create a time averaged potential whose width in modulation direction is 10 times or more the width in the direction perpendicular to it (z). To achieve this it will turn out that one needs roughly the same ratio between modulation amplitude and original beam waist when assuming the original beam to be round (see 3.2.3). That means the experimentally interesting range of values for q are all values above $q \approx \frac{1}{20}$. The larger values of q are interesting as the modulation is used during loading and then will be gradually reduced and turned off before or during the cooling phase.

In figure 4 the potential along the propagation axis is depicted once for the case of the unmodulated potential shown in figure 2 as well as the modulated potential corresponding to figure 3. Here both are shown at the same time so that it is easy to compare the two directly. They both have roughly the same shape, which will be investigated in more depth in the next section, and have their minimum at the same position. One can also observe the lower trap depth here as the peak is smaller by roughly a factor of two at the focus. Interesting here is that this ratio of two between the potentials gets reduced quite fast when increasing $|y|$. This means that there is not just a scaling factor between these two potentials. This is directly clear by thinking about the fact that the beam widens for larger distances $|y|$ from the focus, such that the modulation changes the potential less the further one is away (in propagation direction) from the focus as the modulation amplitude $\hat{x}$ is fixed. How this compares to a Gaussian beam potential with the corresponding beam waists will be investigated in a following section (see 3.2.1)
In figure 5.a) the unmodulated potential as well as the modulated potential used as an example before are shown together with 4 more modulated potentials with different modulation

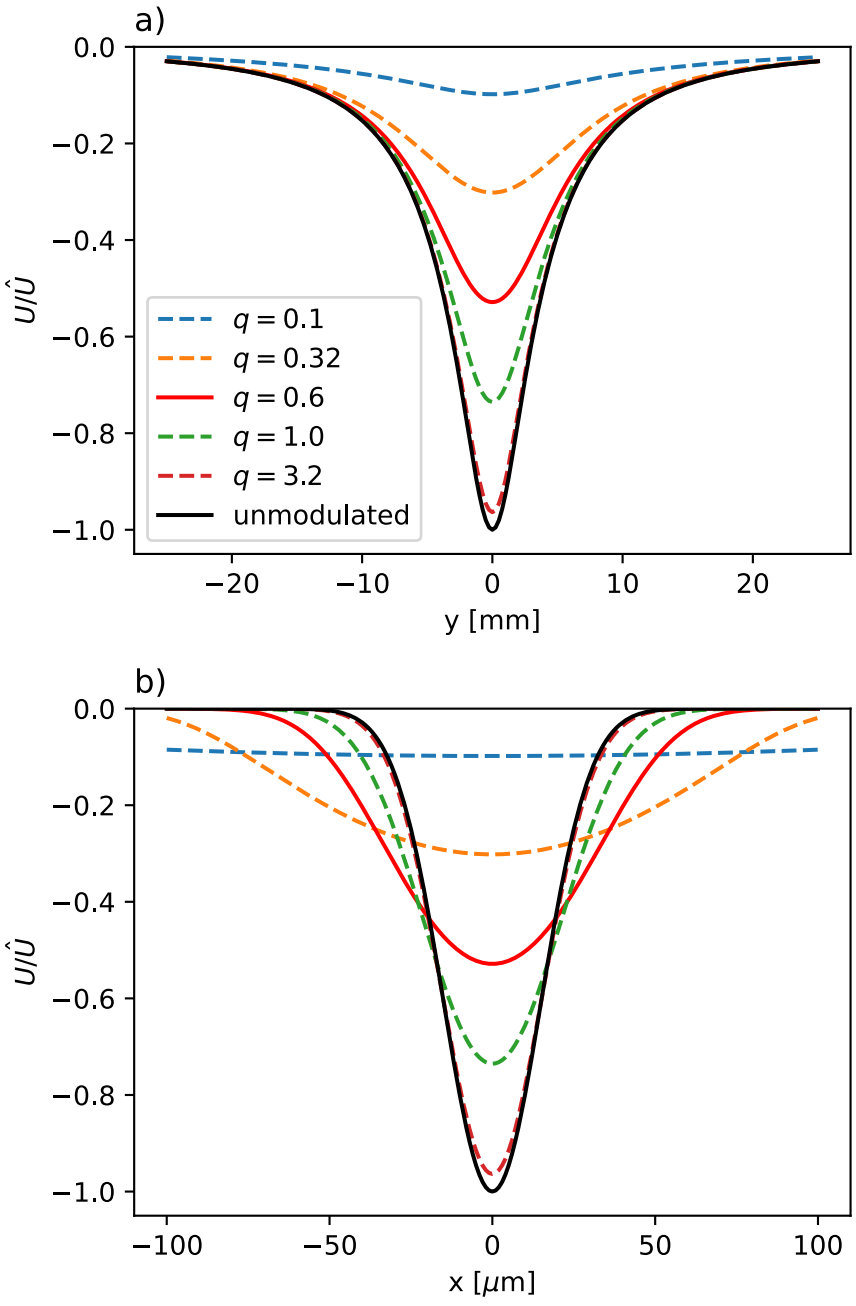

Figure 5: *Plot of potentials with beam waists* $w_x = 30\,\mu\text{m}$, $w_z = 50\,\mu\text{m}$, *power* $P = 10\,\text{W}$ *and modulation with an arccosine (26). The different modulation amplitudes* $\hat{x}$ *are given via* $q = \frac{w_x}{\hat{x}}$. **a)** *along propagation axis,* **b)** *along modulation direction*

amplitudes $\hat{x}$ along the propagation direction y. Here one can clearly see that the effect observed in figure 4 grows larger, the bigger the modulation is compared to the waist in modulation direction of the laser beam. That means for an increasing modulation amplitude the confinement provided by the trap will be decreasing.
In figure 5.b) the same potentials as shown in figure 5.a) are depicted along the modulation direction x. Here one can observe the effect that the width of the potential grows with the modulation amplitude, which is the idea of the tuneable geometry. As the lowering of the trap depth is not a beneficial effect one could for example increase the power of the laser to counteract it.

3.2 Characterisation of arccosine-modulated potential

It is important to know how the time averaged potential can be characterised by the parameters of the Gaussian beam and the modulation. As one has to use numerical integration in the case of the modulation with an arccosine it is not possible to analytically determine the shape of the trap in all directions, with the z-direction being an exception as the integral (see (21)) is in no way dependent on z. To determine the shape of the modulated potential it is first compared to a Gaussian beam potential of the same depth after which the depth and width of the trap will be investigated separately.

3.2.1 Comparison to Gaussian beam potential

First the time averaged potential will be compared to a Gaussian beam potential to see how the shape of the trap changes in the 3 spacial dimensions when it is modulated. More specifically the potential produced by a Gaussian beam given by (7) will be fitted to the modulated potential along propagation (y) and modulation (x) direction. The third dimension z does not require any fits as it, as mentioned before, simply scales with the result of the integral which is independent of z.
Along the two directions x and y the potential is going to be compared for different ratios q of the beam waist in modulation direction w_x to the modulation amplitude $\hat{x}$. A Gaussian beam potential will be fit to the numerically calculated modulated potential for different modulation amplitudes. The only parameter that will be allowed to vary from the parameters of the original beam in the fit will be the beam waist in modulation direction x. By varying additional parameters one can increase the goodness of fit, especially in the central region, but it comes at the cost that then the values of the fitted beam waist for the fits along the two directions may differ. This can be seen for the example of varying power from the fit results $w_x = 69\,\mu\text{m}$ and $w_x = 46\,\mu\text{m}$ presented in figures 7 and 10.

Starting with comparison of the shape along the modulation direction one can see in figure 6 the normalised time averaged potential for $q = \frac{w_x}{\hat{x}} = 1$ and the corresponding fit of the Gaussian beam potential as well as the differences between the two. One can see that the modulated potential can still be described well by a Gaussian potential with the deviations at most ca. 1.2 % relative to the trap depth. It follows that the same is true for larger values of q as this means the modulation has even less effect on the potential.
Therefore the next case to look at is when the modulation amplitude is a bit larger than the beam waist, e.g. two times the beam waist which is depicted in figure 7. Here one can already clearly see the deviations between the two potentials by eye and said deviations

reach values of up to 5 %. At this point it is clear to see this is no longer a perfect Gaussian potential.
This can be seen more clearly for even smaller values of q, for example $q = \frac{1}{10}$ as shown in figure 8. Here the potential seems to get closer to a parabola than a Gaussian potential.
For extreme values of q it does not transform to an harmonic potential as it is too wide, but the edge at $|\tilde{x}| = \left|\frac{x}{\hat{x}}\right| = 1$ gets harder (see B.2 - figure 35). This means that one could define the trap size for large modulation amplitudes solely via the modulation amplitude $\hat{x}$, which will be investigated in the respective section (see 3.2.3).

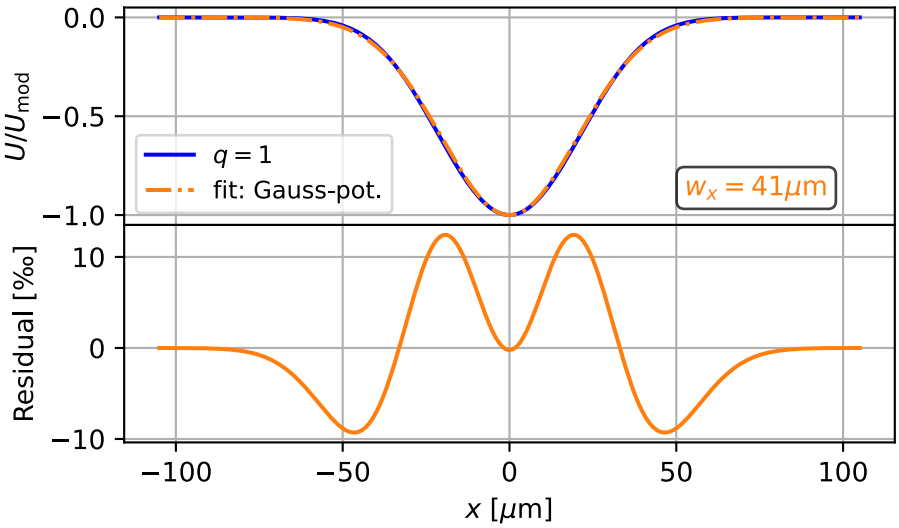

Figure 6: *Comparison of a time averaged potential (original beam waist $w_x = 30\,\mu$m) with $q = 1$ and a fitted Gaussian beam potential along the modulation direction ($y = z = 0$). The fit function (7) has all values but w_x fixed to the same values as the modulated potential.* **Top***: Plot of the potentials normalised to the trap depth of the modulated potential;* **Bottom***: Plot of the differences between the normalised potentials ($U_{\mathrm{fit}} - U_{\mathrm{mod}}$).*

Turning to the shape along the propagation direction y there is an interesting phenomenon, as the shape of the time averaged potential can be described well by an unmodulated potential not only for large q but also for small q. Only in the range in which the experiment will work (ca. $q \geq \frac{1}{20}$ as mentioned before in 3.1.1) the modulated potential is not as easily described by an Gaussian beam potential, when only using the beam waist w_x as parameter. By allowing the power to vary as well one can reach a much higher agreement with the modulated potential although the downside is that one produces inconsistent fits for the different directions. Thus when using this to describe the potential along the propagation direction one has to make sure to not use it on any other direction as this wouldn't produce correct results (compare figures 7&10). As one can see in figure 10 the modulated potential is actually narrower than a Gaussian beam potential of the same depth when only w_x changed. What this also implies is that with a Gaussian beam potential the same trap shape along the propagation direction can be achieved with (in this case) only 70 % laser power. This is of course an effect of the widening of the trap in modulation direction which is not visible here. Hence there needs to be effectively less power along one specific axis (here $x = z = 0$) as the power is more broadly distributed.

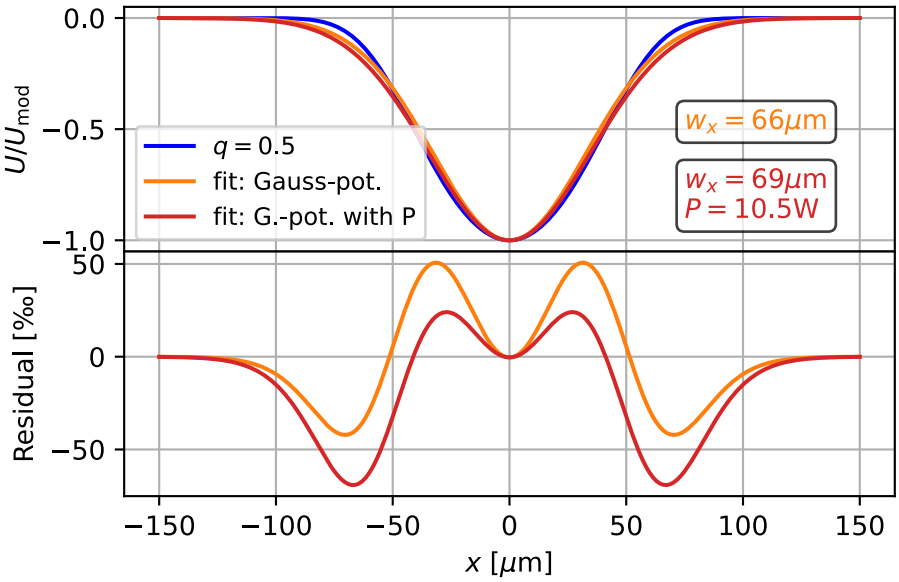

Figure 7: *Comparison of a time averaged potential (original beam: $w_x = 30\,\mu$m, $P = 10\,$W) with $q = \frac{1}{2}$ and a fitted Gaussian beam potential along the modulation direction ($y = z = 0$). The fit function (7) has all values but w_x (and P) fixed to the same values as the modulated potential. The only difference between the orange and red fit is the fact that for the orange fit the power is fixed to $P = 10\,$W. Both fits have been given larger weights for the central region of the potential.* **Top**: *Plot of the potentials normalised to the trap depth of the modulated potential;* **Bottom**: *Plot of the differences between the normalised potentials ($U_{\mathrm{fit}} - U_{\mathrm{mod}}$).*

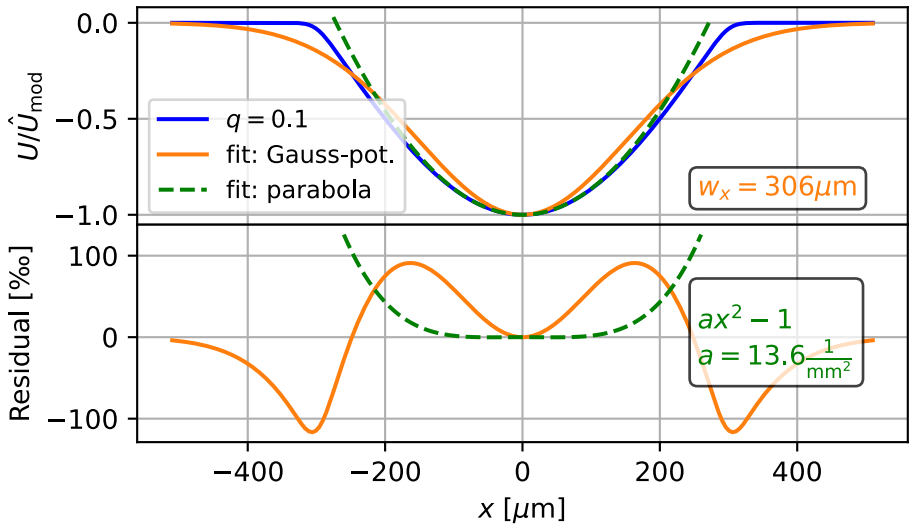

Figure 8: *Comparison of a time averaged potential (original beam waist $w_x = 30\,\mu\mathrm{m}$) with $q = \frac{1}{10}$ and a fitted Gaussian beam potential as well as a parabola along the modulation direction ($y = z = 0$). The fit function (7) has all values but w_x fixed to the same values as the modulated potential. Note that the parabola is just fit to the central region of the potential.* **Top**: *Plot of the potentials normalised to the trap depth of the modulated potential;* **Bottom**: *Plot of the differences between the normalised potentials ($U_{\mathrm{fit}} - U_{\mathrm{mod}}$).*

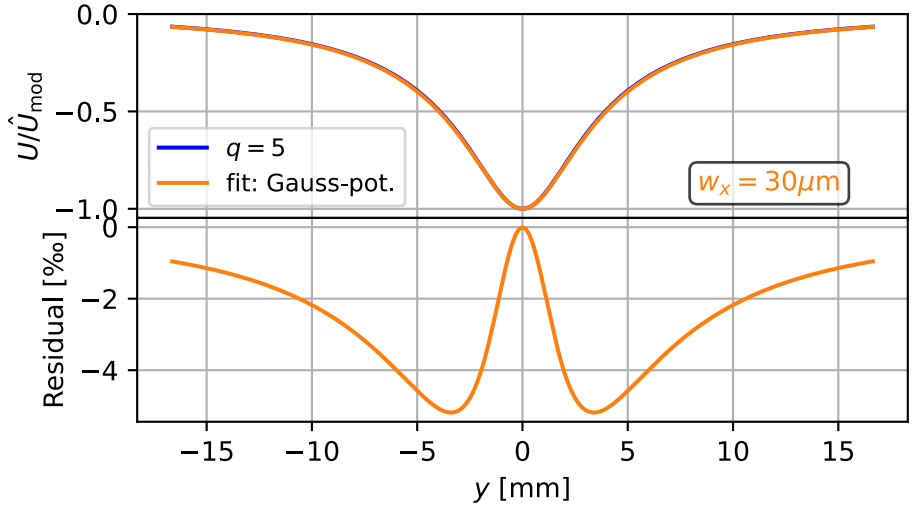

Figure 9: *Comparison of a time averaged potential (original beam waist $w_x = 30\,\mu\mathrm{m}$) with $q = 5$ and a fitted Gaussian beam potential along the propagation direction ($x = z = 0$). The fit function (7) has all values but w_x fixed to the same values as the modulated potential.* **Top**: *Plot of the potentials normalised to the trap depth of the modulated potential;* **Bottom**: *Plot of the differences between the normalised potentials ($U_{\mathrm{fit}} - U_{\mathrm{mod}}$).*

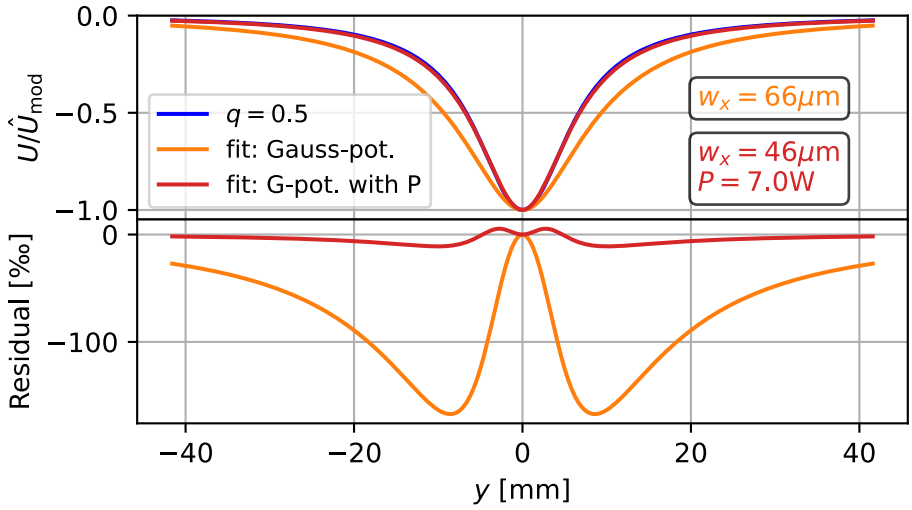

Figure 10: *Comparison of a time averaged potential (original beam waist $w_x = 30\,\mu\mathrm{m}$, power $P = 10\,\mathrm{W}$) with $q = \frac{1}{2}$ and a fitted Gaussian beam potential along the propagation direction ($x = z = 0$). The fit function (7) has all values but w_x (and P) fixed to the same values as the modulated potential.* **Top**: *Plot of the potentials normalised to the trap depth of the modulated potential;* **Bottom**: *Plot of the differences between the normalised potentials ($U_{\mathrm{fit}} - U_{\mathrm{mod}}$).*

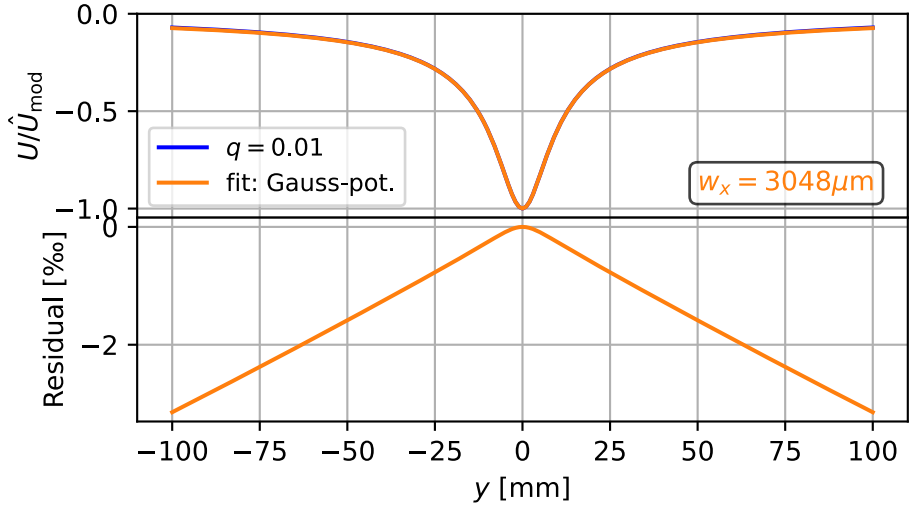

Figure 11: *Comparison of a time averaged potential (original beam waist $w_x = 30\,\mu\mathrm{m}$) with $q = \frac{1}{100}$ and a fitted Gaussian beam potential along the propagation direction ($x = z = 0$). The fit function (7) has all values but w_x fixed to the same values as the modulated potential.* **Top**: *Plot of the potentials normalised to the trap depth of the modulated potential;* **Bottom**: *Plot of the differences between the normalised potentials ($U_{\mathrm{fit}} - U_{\mathrm{mod}}$).*

Lastly to note is the fact that in the z-direction nothing changes from the unmodulated Gaussian apart from the trap depth as the integral is constant if z is the only variable and hence only works as a scaling factor for the potential. A fit with only w_x as parameter would produce exactly the same result for w_x as in the other two directions as there is only one value for w_x that correctly scales the potential.

3.2.2 Trap depth

The first parameter of the trap that will be investigated is the trap depth, more specifically how the trap depth (relative to the trap depth of the unmodulated potential) changes with the modulation amplitude. For an arbitrary modulation function one would first need to determine the position of the minimum as it can be moved away from the original beam focus e.g. when modulating with a sine-wave. In the case of modulation with an arccosine the potential minimum always stays at the same position (i.e. $x, y, z = 0$), which means any relative difference in trap depth can simply be determined by evaluating the integral:

$$\frac{\hat{U}_{\text{mod}}}{\hat{U}} = \frac{1}{T}\int_0^T \exp\left(-2\frac{\xi^2(t)}{q^2}\right) \mathrm{d}t \tag{32}$$

$$= \frac{-\pi}{4}\int_{-1}^{+1} \cos\left(\frac{\pi}{2}\mu\right) \exp\left(-2\frac{\mu^2}{q^2}\right) \mathrm{d}\mu \tag{33}$$

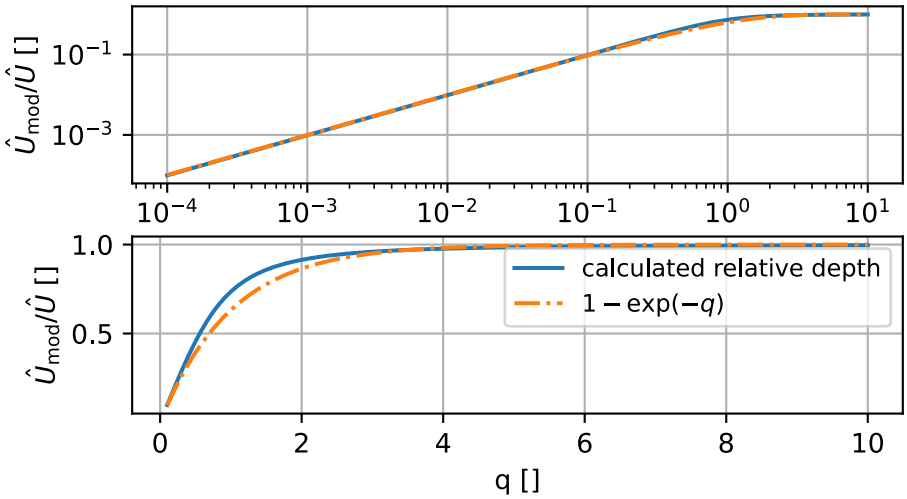

Figure 12: *Plot of the trap depth relative to the unmodulated potential for a modulation with an arccosine. Additionally the function $f(q) = 1 - \exp(-q)$ is plotted.* **Top***: double-logarithmic plot for $q \in [10^{-4}, 10]$;* **Bottom***: cartesian plot for $q \in [0.1, 10]$*

This expression does not have an analytical solution and has to be integrated numerically. As the position is fixed, the only parameter the integral depends on is $q = \frac{w_x}{\hat{x}}$ and one can easily calculate the relative trap depth for a range of values for q. In figure 12 this is shown for the range $q \in [10^{-4}, 10]$, where one can also see that the relatively simple function $f(q) = 1 - \exp(-q)$ provides a somewhat similar shape with suitable limits. These limits are $\frac{\hat{U}_{\text{mod}}}{\hat{U}} = 1$ for $q \to \infty$ and $\frac{\hat{U}_{\text{mod}}}{\hat{U}} = q$ for $q \to 0$. Unfortunately the function fails to describe

the region around $q = 1$, which is quite interesting for this experiment. One can experiment with modifying $f(q)$ by adding parameters and then fit it to the interesting region, but no simple modification produced great results. Looking for a more sophisticated function to describe this would take time and not provide a great benefit as the numerically calculated values show the shape very clear and specific values can be easily calculated.

3.2.3 Trap width

Next to the trap depth the most important characteristic is the trap width, that is to say in which space the trapped atoms are confined. As the time averaged potential generated with an arccosine-modulation is still close but not equal to a Gaussian beam potential the trap width will be characterised via the full width at half maximum (FWHM) and/or the trapping frequencies in case of an harmonic approximation. As the calculation of both of these values turns out to be quite difficult for the x- and y-directions they will be determined numerically. For the z-direction this is not necessary as the integral is not dependent on z, which means the trap in z-direction still follows the same formulas as before with the depth modified. The FWHM_z is not affected at all and is given as

$$\mathrm{FWHM}_z(w_z) = w_z\sqrt{2\ln(2)} \tag{34}$$

The trapping frequency ω_z in z-direction still follows (15) but as the trap depth decreases the trapping frequency decreases as well.

We now focus on the FWHM in modulation direction x which is shown as a function of q in figure 13. The limit for large values of q is obviously the value of the unmodulated potential which can be seen well in figure 13.a). For the limit of small q on the other hand it is reasonable to assume that the shape of the beam loses in significance against the modulation function as the modulation dominates the shape of the time averaged potential. This leads to the assumption of a linear relation to the modulation amplitude instead of the beam waist which can best be seen in 13.b). The proportionality factor seems to approach $\frac{4}{3}$ fast for small q, which was determined via fitting a straight line.
As the determination of the FWHM_x requires more than just numerically evaluating an integral it would be nice to have a function to get a good estimate of the trap width. For this reason a fit in the transition area was performed with the results on display in 13.c). This range of values for q is in fact one that is interesting for the experiment. So here one can use

$$\mathrm{FWHM}_x \approx \hat{x}\cdot\left[1.35 + \frac{(q-0.392)\sqrt{2\ln(2)}}{1+\left|(q-0.392)\sqrt{2\ln(2)}\right|^{-1}}\right] \tag{35}$$

to get a good estimate of the trap width for $0.2 < q \lessapprox 4$. In fact the limit for large q is not very far off as the slope is correct but the approximation will have an offset of ca. $-0.2\cdot\hat{x}$ compared to the real function.
A simpler function with the correct limit on both sides would be

$$\mathrm{FWHM}_x \approx \sqrt{\frac{16}{9}\hat{x}^2 + 2\ln(2)w_x^2} \tag{36}$$

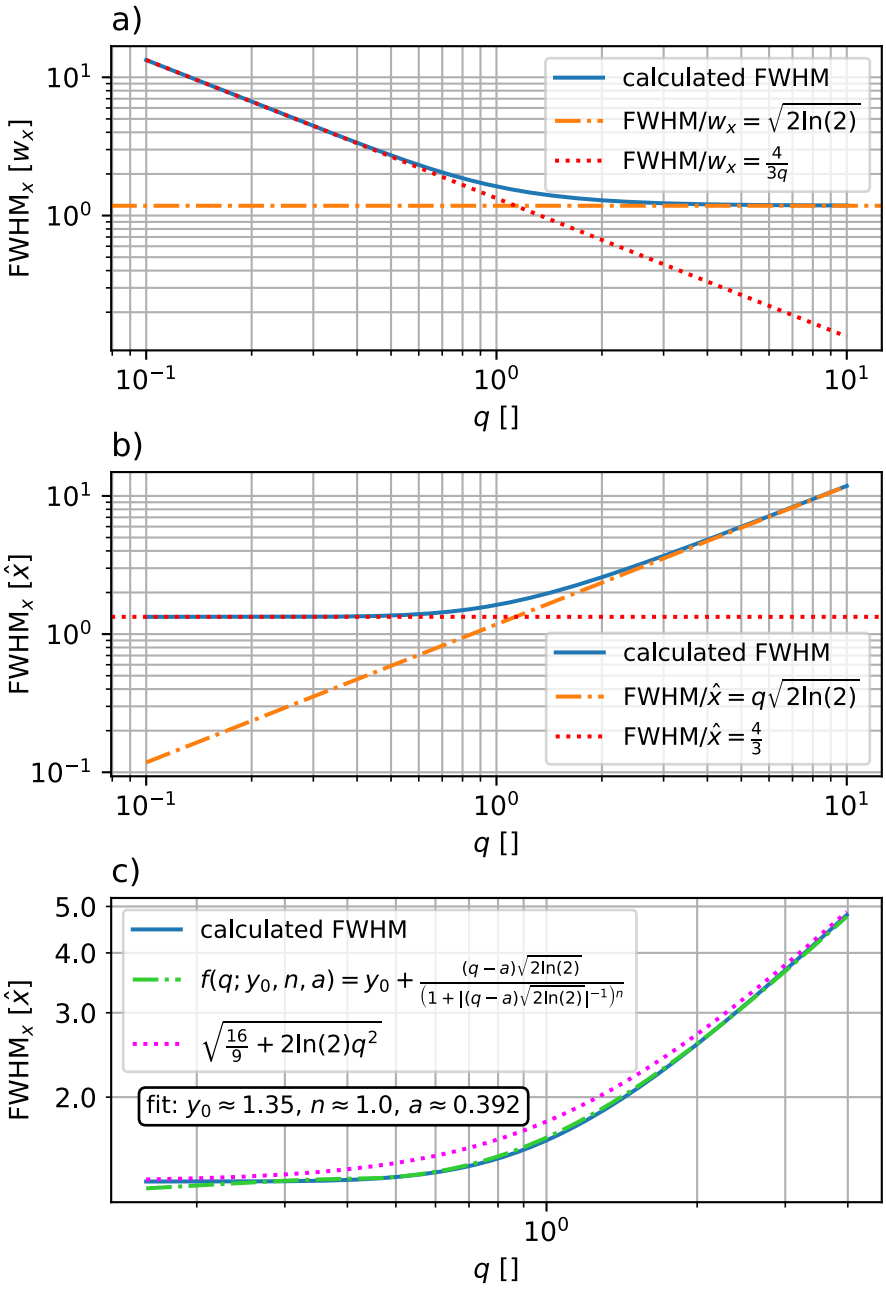

Figure 13: *Plots of the FWHM in units of the orignial beam waist w_x or modulation amplitude $\hat{x}$ in modulation direction with respect to q.* **a)** *The FWHM is given in units of w_x which means to limit for large q, i.e. an unmodulated potential is given as $\sqrt{2\ln(2)}$. The limit for small q was acquired with the help of a fit.* **b)** *Here the FWHM is given in units of the modulation amplitude $\hat{x}$ to illustrate the limits from a) in a different way.* **c)** *For the transition area a fit to the FWHM was performed. This fitted function produces good results in the desired range but will deviate fast for smaller q. The other function given provides the right limits but as one can see does not describe the region around $q = 1$ very well.*

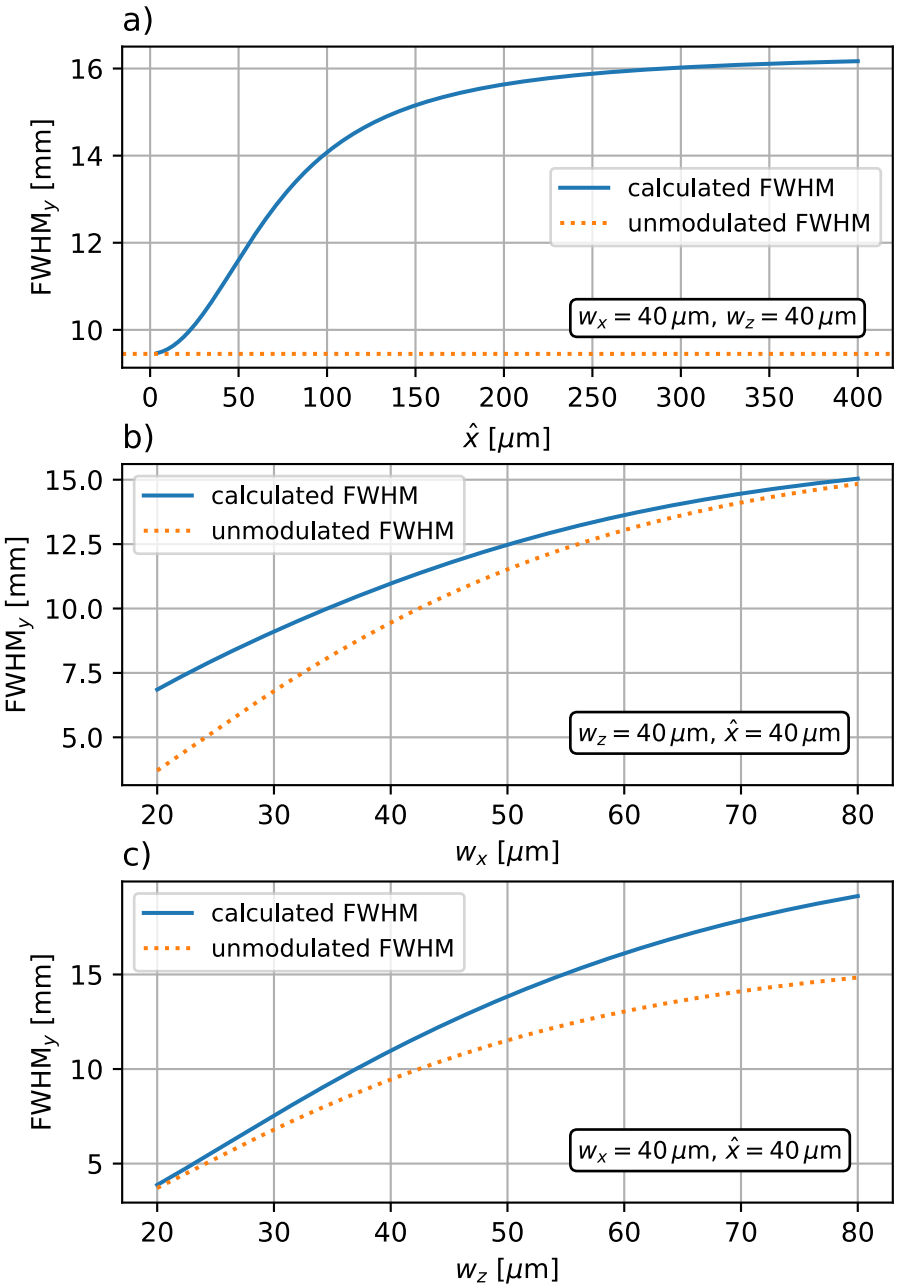

Figure 14: *Plots of the FWHM in propagation direction with respect to the varied parameter ($\hat{x}$, w_x or w_z). As base value for all three parameters 40 µm was arbitrarily chosen. Additionally to the calculated FWHM of the modulated potential the FWHM of the unmodulated potential is shown for comparison.* **a)** *The modulation amplitude is varied such that $q \in [0.1, 10]$.* **b)** *The beam waist in modulation direction is varied such that $q \in [0.5, 2]$* **c)** *The beam waist perpendicular to the modulation direction is varied such that $\frac{w_z}{\hat{x}} \in [0.5, 2]$*

As here the deviations in the region of $q \approx 1$ are larger than those of (35) it may serve as a simpler but also less exact estimation in the region of interest.

The trapping frequencies can then either be determined via a parabolic fit to a specific potential like it was done in 8 but this would require a large amount of computation if you were interested in many values. Therefore as an estimate one can also assume the potential to be harmonic and calculate the trapping frequencies from the FWHM and the trap depth:

$$-\frac{1}{2}\hat{U} = -\hat{U} + \frac{1}{2}\left(\frac{\mathrm{FWHM}_x}{w_x}\right)^2 = -\hat{U} + \frac{1}{8}m\omega^2\mathrm{FWHM}_x^2 \tag{37}$$

$$\Rightarrow \omega^2 = \frac{4\hat{U}}{\mathrm{FWHM}_x^2 m} \tag{38}$$

$$\Rightarrow \omega = \frac{2}{\mathrm{FWHM}_x}\sqrt{\frac{\hat{U}}{m}} \tag{39}$$

Note that this underestimates the trapping frequencies, as a harmonic potential, that describes the central part of the potential well, would have a smaller FWHM than a Gaussian potential or the time averaged potential. This can be seen by assuming the unmodulated potential as the trapping frequency would then be underestimated by a factor of

$$\frac{\omega_{x,\mathrm{unmod}}}{\omega_{x,\mathrm{estimate}}} = \frac{\mathrm{FWHM}_x}{w_x} = \sqrt{2\ln(2)} \approx 1.18 \tag{40}$$

This factor will shrink for larger modulation as the potential gets wider (see figures 6-8). If the modulation is not large it is thus better to assume the modulated potential to be a Gaussian and use

$$\omega = \frac{2}{\mathrm{FWHM}_x}\sqrt{\frac{2\ln(2)\hat{U}}{m}} \tag{41}$$

Regardless which formula is used it is obvious that for a lower trap depth the trapping frequencies decrease at least as fast as in (15) or faster when the modulation amplitude increases. This is clear as the trapping frequencies still scale with the trap depth $\omega \propto \sqrt{\hat{U}}$ but now the length scale is no longer fixed to w_x but increases with the FWHM as seen in figure 13. Hence the trapping frequencies additionally drop with the rising FWHM as $\omega \propto \frac{1}{\mathrm{FWHM}_x}$.

For the propagation direction a fit turns out to be somewhat difficult in general as the shape of the potential in y-direction can not be simplified as easily as for the other directions due to the fact that y is a parameter in every part of the function. The integral as well as the factors multiplied to it depend on y which makes it impossible to assume that q as the only parameter could determine the FWHM. This is also clear to be seen from figure 14.c) as even for constant q the trap width varies with w_z. Determining the shape of the trap along the propagation direction in greater detail surpasses the scope of this thesis.

3.3 Acousto-Optic Deflector

An acousto-optic deflector (AOD) allows control over the direction, frequency and intensity of a laser beam. This is done by varying the frequency and amplitude of the signal which

drives the AOD. Varying the amplitude of the signal has little effect on the direction or frequency of a laser beam whereas the frequency of the driving signal influences all three mentioned aspects of the beam.
The difference in use between an AOD and an acousto-optic modulator (AOM) is the fact that AODs are specifically geared towards deflection of the beam with very little influence of the signal frequency on the beam intensity. This is done by increasing the bandwidth of the AOD in comparison to the AOM. That means the AOD works with a larger range of driving frequencies and thus can deflect light for a larger range of angles with good diffraction efficiency.
The information presented in this section about AODs and AOMs can be found in [McC07] and [ST91, chapter 20].

3.3.1 Working principle

Central to every AOD is a crystal in which sound waves are induced. AODs and AOMs work in a very similar way with, in our case the only difference being that the sound waves in our AOD are not generated by a single piezoelectric element but by two phase-shifted piezoelectric elements.[3]
The basic principal is to generate periodic sound waves that modulate the density and thus also the refractive indices of the crystal. By this periodic modulation of refractive indices, i.e. the generation of a thin diffraction grating, the crystal then scatters the incident light into different orders $m \in \mathbb{Z}$. The scattered light then interferes constructively at an angle θ with the Bragg condition for the constructive interference where the angles of the incident and deflected light being the same angle θ:

$$m\lambda = 2\Lambda \sin(\theta) \tag{42}$$

with the optical wavelength λ and the acoustic wavelength Λ. This is only the result of an approximation for the case $\lambda \ll \Lambda$ as it ensures that one period of the sound wave is small enough compared to the period of the light such that assuming the grating induced in the crystal is static becomes a good approximation . This is generally the case (by at least five orders of magnitude) so it does not need further attention.
Another effect that comes together with the deflection of the light is a slight energy shift of the light. This can be described via the Doppler-effect as the light is reflected off of a moving wave with velocity $v_s = \frac{\Lambda\Omega}{2\pi}$ which has the angular frequency Ω such that the resulting frequency of the light is given by

$$\begin{aligned} \omega_d &= \omega\left(1 + 2\frac{v_s}{c}\sin(\theta)\right) \\ &= \omega\left(1 + 2\frac{\Lambda\Omega}{2\pi}\cdot\frac{2\pi}{\lambda\omega}\cdot\frac{m\lambda}{2\Lambda}\right) \\ &= \omega + m\Omega \end{aligned} \tag{43}$$

One can also see from (42) how one can control the angle of the diffraction order by changing the driving frequency for the sound waves as $\Lambda = \frac{v_s}{f_{\text{drive}}}$ such that $\sin(\theta) \propto f_{\text{drive}}$.
Here one can also find the reason as to why the angles are controllable and why there is a

[3] Note that there is not one single AOD design and thus another AOD may be built in a different way but the simple explanation provided here should be correct independent of the concrete model used.

non-zero bandwidth for an AOD. The reason for this is that the Bragg angle changes with the wavelength of the sound waves, i.e. the frequency of the driving signal. As the Bragg angle changes (see 42) with the frequency of the sound wave, but the angle of the incident light relative to the sound waves stays the same, the diffraction into the respective order drops rapidly. It would even drop to zero instantly if both sound and light could be described as planar waves. As this is not the case one still diffracts light into said order even if the angle is slightly off.
An AOD optimises the diffraction efficiency over a large range of frequencies to provide a large bandwidth. In our case this is achieved by cleverly creating sound waves with a larger spread of directions while carefully making sure that this does not affect the maximal diffraction efficiency too much. This allows a larger amount of incident light to have the correct angle with respect to some sound wave and thus allowing the incident light to be diffracted into the respective order.

The quantum interpretation of these effects is done via the interaction of an incident photon (momentum $\hbar\mathbf{k}$, energy $\hbar\omega$) with m phonons (momentum $\hbar\mathbf{q}$, energy $\hbar\Omega$) in the crystal. Using the conservation of momentum leads to the wavevector $\mathbf{k}_d$ of the deflected light being determined by

$$\mathbf{k}_d = \mathbf{k} + m\,\mathbf{q} \tag{44}$$

with $\mathbf{k}$ the wavevector of the incident light and $\mathbf{q} = \frac{2\pi}{\Lambda}\hat{\mathbf{q}}$ the wavevector of the phonon. The conservation of energy on the other hand directly leads to equation (43). For $m > 0$ this corresponds to the photon absorbing m phonons whereas $m < 0$ means that the photon induced $|m|$ phonons in the crystal.

3.3.2 Diffraction efficiency into the 1^{st}-order

The usual mode of operation which will also be used in this thesis is to optimise the intensity of the first diffraction order. To be able to characterise this optimisation independent from the incident intensity one does not look at the absolute value of the intensity in the first order but at the so called diffraction efficiency which is defined as the ratio of intensity of the deflected light and the incident light.
For this it is important to know how the diffraction efficiency in the first order depends on the parameters that can be controlled. The diffraction efficiency into the first order (m=1) with the incident light at the Bragg angle is given by:

$$\begin{aligned} DE &= \sin^2\left(\sqrt{2\pi^2 n^2 \frac{L^2\Lambda^2}{\lambda^4}\mathcal{M}I_s}\right) \\ &\overset{\sqrt{\cdot}\ll 1}{\approx} 2\pi^2 n^2 \frac{L^2\Lambda^2}{\lambda^4}\mathcal{M}I_s \end{aligned} \tag{45}$$

n is the refractive index of the material, L is the length of the crystal (in direction of the sound wave propagation) and $\mathcal{M}$ is a material parameter which depends on the polarisability, the refractive index, the density and the sound speed of the material.

When **setting up an AOD in practice** one will have chosen a laser and AOD for the set-up beforehand and thus everything but the signal send to the AOD is already fixed. Therefore

one has only this driving signal and the positioning to control the diffraction efficiency.
Concerning the driving signal one has to be a bit careful about the driving frequency $f_s = \frac{\Lambda}{v_s}$ as AODs have a center frequency that they are built around where they perform the best, thus one cannot freely adjust the frequency of the sound. One has to rely on the intensity, i.e. the amplitude of the driving signal to optimise the diffraction efficiency.
The first step is to connect the AOD to the driving signal source with the frequency set to the center frequency or something close to it and a reasonably high amplitude so that diffraction orders are visible when directing the beam through the AOD. With this the AOD has to be turned to the correct angle for diffraction into the first (or minus first) order. As this angle is very narrow for a given sound frequency one has to do very small adjustments. The goal is here to have the intensity in the first order at least comparable to the intensity in the zeroth order to be able to further adjust it afterwards. When this is done one can tune the intensity of the signal to maximise the intensity of the beam into the first order. If everything is set-up well one should be able to reach a diffraction efficiency around 80 % to 90 %.

Regarding the diffraction efficiency of our AOD in dependence on the driving frequency one has two vastly different situations depending on the phase difference that is applied between the two inputs of the AOD. In the case that the additional phase is applied to the right input (which was found to be the input on the side of the incident light here) one receives the profile of stable high diffraction efficiency that the AOD is made for. In the case that the phase difference is inverted one seems to get the diffraction efficiency profile of a regular AOM, which is unwanted in this context as it does not allow for large modulation due to it's low bandwidth.

4 Experiment - Set-up

4.1 Electronic circuit for AOD

To use the AOD[4] one needs to provide the driving RF-signal and produce the correct phase difference after splitting it. The power splitter[5] with cables producing the needed phase difference were delivered with the AOD, the difference in cable length being 2.461 m.
The circuit for the RF-signal is where the modulation is generated and it is also the main reason why the modulation frequency has an upper limit (see section 4.1.1). The required parts for this circuit are a voltage controlled oscillator (VCO)[6], an arbitrary function generator (AFG)[7], a mixer[8] (or a voltage controlled attenuator), a power splitter and two amplifiers[9]. A VCO produces a sine-wave of a given frequency, which can be controlled by the function generator. The conversion of the applied voltage on the VCO to frequency of the signal can be approximated as linear. This signal from the VCO is fed to a mixer, which regulates the power of said signal by applying a DC control voltage. After that the signal is split by a power splitter and accumulates a phase difference by going through different lengths of cable to the amplifiers. The amplifiers should have the same gain and thus tunable amplifiers would be somewhat impractical here. The amplified signals are then fed to the AOD. This circuit is depicted in figure 15. Here one has to be careful of where one connects the cables as the phase difference has to be in the right direction. Failing to do so will result in the diffraction efficiency being very similar to the one of an AOM which means there is a much lower bandwidth for the modulation. In this experiment the correct order was found to be the longer cable, i.e. the signal with more accumulated phase, closer to the incident beam. For figure 15 this would for example mean that the light would have to travel upwards in the picture plane.

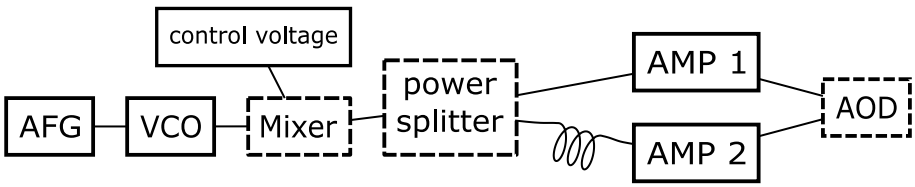

Figure 15: *The circuit for the generation of the AOD driving signal. The nodes with uninterrupted frames are components that require additional power supply that is not shown here.*

4.1.1 Limitations

Limitations of this set-up mainly concern the modulation frequency and amplitude. The VCO takes an input voltage from 1 V to 16 V but the AFG can only output up to 10 V. As here there is no additional amplifier connected between the two the output of the VCO is limited. This then of course also limits the diffraction bandwidth of the AOD driven by the signal

[4] AOD model: Gooch&Housego 4075-2
[5] power splitter model: Mini-Circuits ZFSC-2-1-S+
[6] VCO model: Mini-Circuits ZOS-100
[7] AFG model: Rigol DG4162
[8] mixer model: Mini-Circuits ZX05-5-S+
[9] AMP model: Mini-Circuits ZHL-1-2W

produced. This is not a major problem as the range of frequencies where the AOD provides the highest diffraction efficiencies is still accessible but it does still provide a limit for the modulation amplitude.

The frequency output of the VCO as well as the corresponding diffraction efficiency (DE) of the AOD are shown in figure 16. One can see that the frequency output of the VCO has a linear dependence on the AFG voltage whose parameters were determined by a fit and are depicted in figure 16. Further one can see that the DE has two local maxima or a plateau in the center and drops off to the edges of the plot. The mean diffraction efficiency of 86 % was determined from the data points shown here which is good for a width of 36 MHz. The AOD is specified to have a center frequency of 75 MHz which corresponds to an AFG voltage of ca. 7.6 V and the right maximum of the DE in figure 16. This is not in the center of the diffraction efficiency curve seen here and thus doesn't result in the largest possible bandwidth. Therefore for this experiment a center frequency corresponding to 6 V AFG voltage, i.e. ca. 68 MHz, was chosen as this also allows to make the most of the limited voltage range of the AFG.

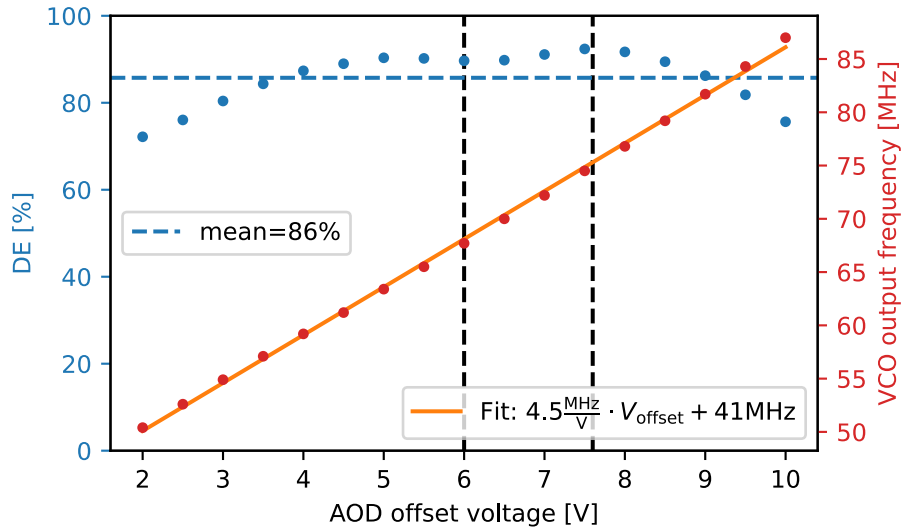

Figure 16: *Plot of the diffraction efficiency (DE) and the VCO output frequency in dependence on the AOD voltage without modulation. For the DE the mean is shown and for the frequency output a linear fit was performed and is displayed. The AOD is specified to work in the frequency range* 59 MHz *to* 91 MHz *which makes the center frequency* 75 MHz *(right vertical line) and the bandwidth* 32 MHz*. Due to the result shown here a center frequency of ca.* 68 MHz *at the offset of* 6 V *(left vertical line) was determined to be more suitable. The maximal used range in this experiment corresponds to the range depicted here, which is* 2 V *to* 10 V *or (for small modulation frequency)* 50 MHz *to* 86 MHz*.*

Concerning the modulation bandwidth the VCO itself has a bandwidth for modulation of 100 kHz[10], which means one has to stay below that, as a high modulation frequency will lead to a reduction in modulation amplitude. Depending on the bandwidths of the electronics

[10] This is defined by the modulation frequency where the output power is reduced by 3 dB.

around the VCO a significant reduction can also happen earlier. Therefore one has to check the bandwidth of the set-up before using it to be sure it is working as intended.

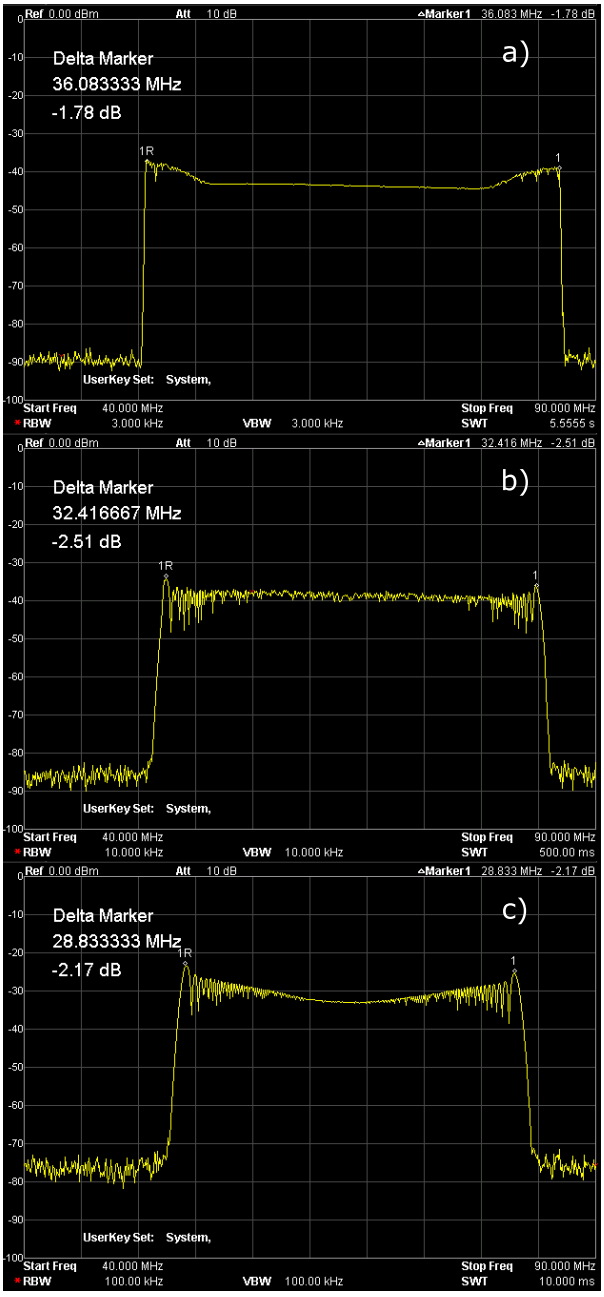

Figure 17: *Pictures of the VCO output for the modulation with a ramp-function with the tuning voltage of the VCO at* $6\,\mathrm{V} \pm 4\,\mathrm{V}$ *for different modulation frequencies.* **a)** *modulation frequency*=0.5 kHz **b)** *modulation frequency*=25 kHz **c)** *modulation frequency*=50 kHz

Regarding the bandwidth the circuit presented here was tested for the relevant modulation frequencies from 0.5 kHz up to 50 kHz. The used offset for the modulation function fed to the VCO is 6 V with a modulation with a ramp (linear) function using an amplitude of $\pm 4\,\mathrm{V}$.

For 0.5 kHz, 25 kHz and 50 kHz the frequency output of the VCO is depicted in figure 17. It was measured by connecting the auxiliary output of the VCO to a spectrum analyser[11]. One can see that in all three pictures the frequency range that is reached with the VCO is clearly elevated from the background. In all three pictures one can also see that there seems to be a bit more intensity at the edges of the range, which is not expected for a ramp function as it is supposed to be uniform. There are also noticeable differences in the frequency output between the three measurements: The edges of the frequency range become less sharp and the range shrinks in size for an increasing modulation frequency. With the range of the modulation amplitude of the frequency reducing from 36.1 MHz over 32.4 MHz to 28.8 MHz it is clear that there is already some noticeable reduction of the modulation amplitude $\hat{x}$. In the range where the modulation frequency will be chosen for the actual experiment the modulation range is already reduced by over 10 %. This is not great, but it also is not terrible as it simply means that the modulation amplitude is scaled down slightly since the modulation frequency remains fixed during operation.

4.1.2 Issue with arccosine-modulation

Modulating with other standard functions of the function generator (sine or square) produces similar results but modulating with an arccosine-function produced an unexpected behaviour at the higher modulation frequencies which can be seen in figure 18.a). There one can see a peak at the edge of the modulation range which should not exist. The same shape is shown in figure 18.b) for a smaller modulation frequency and amplitude although here it is not as strong. In both cases one can see a clear asymmetry between the edges as the one towards lower frequencies is not very sharp whereas the one towards higher frequencies is a clear cut for both edges. Lower amplitude at the edges of the modulation range is expected for an arccosine-modulated tuning voltage as this means the voltage is at the maximum/minimum only for a very short time. This should thus be visible in the spectrum analyser as lower amplitude for the corresponding frequencies as it is approximately seen in figure 18.b) for the low frequencies.

To get an idea what shape one would expect theoretically we will follow a simple argument. We assume that the amount of time that a specific value y of the modulation function is held is proportional to the amplitude of the frequency corresponding to y as it simply allows for power to go towards that specific frequency. This time is then inversely proportional to the derivative of the modulation function at the point y. To see this one can linearise the function in the point y such that a time interval Δt is given by

$$\Delta t = \left| \frac{\Delta y}{\xi'(t)} \right| \tag{46}$$

for an arbitrary value of Δy. Thus the shape for the amplitude in dependence on the frequency $f \propto y$ is the same as the absolute value of the inverse of the derivative of the modulation function in dependence on the function value y, which can be seen in figure 19. Both axis would of course need to be transformed to fit the dimensions of frequency and amplitude.

[11] spectrum analyser model: Rigol DSA705

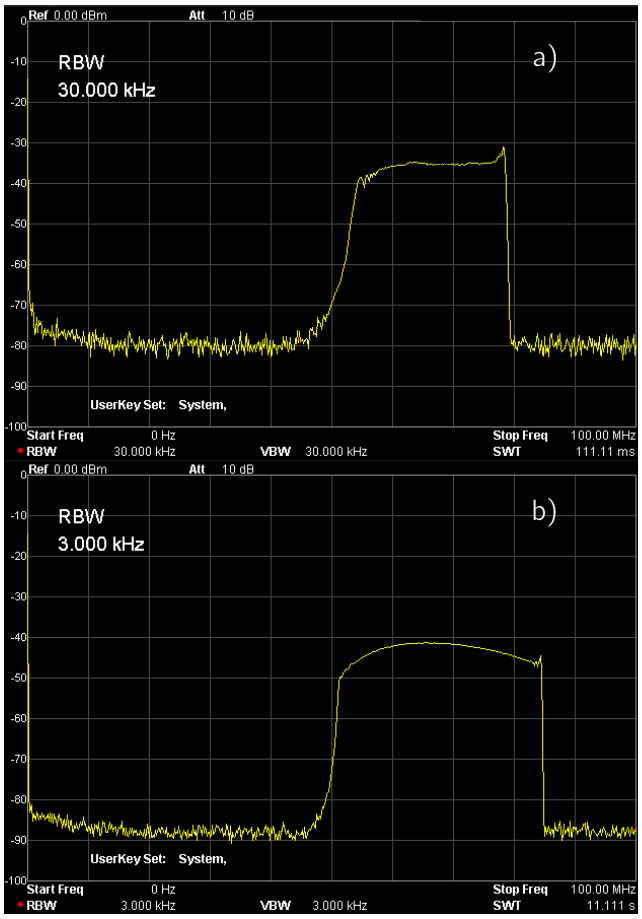

Figure 18: *Pictures of the VCO output for the modulation with an arccosine-function with the tuning voltage of the VCO modulated around* 6 V *with* ±4 V. **a)** *modulation with* 25 kHz **b)** *modulation with* 0.5 kHz

The function that is plotted is given by

$$\frac{1}{|\xi'(t(y))|} = \frac{T\pi}{4}\sqrt{1-\cos^2\left(\frac{\pi}{2}(y+1)\right)} \tag{47}$$

$$= \frac{T\pi}{4}\cos\left(\frac{\pi}{2}y\right) \tag{48}$$

As only the function generator and the VCO produce the signal shown here one of them has to be the source of the issue. To check for an effect of the function generator the produced signal was looked at via an oscilloscope[12] in a range of 1 kHz to 100 kHz. There were no obvious differences observed in the waveform as one can see in figure 20, hence the assumption is that the VCO is the source of this issue.
Another way to assure oneself that the used function generator is appropriate is to look at the sample rate that was stated at $5 \times 10^8\,\mathrm{s}^{-1}$ for the used function generator. This means for a modulation frequency of 25 kHz as in figure 18.a) one would have 2×10^4 sample points per period of the modulation function. Such an amount of sample points should provide enough

[12] oscilloscope model: Rigol DS1104

accuracy to correctly model the function and especially not allow large errors as seen in the signal after the VCO. Therefore one can be sure that the VCO is the reason for these errors. As there was no other available VCO for the required frequency range and not sufficient time for an order to arrive after this issue was found it was not investigated further and a lower modulation frequency was used for the following measurements in this thesis.

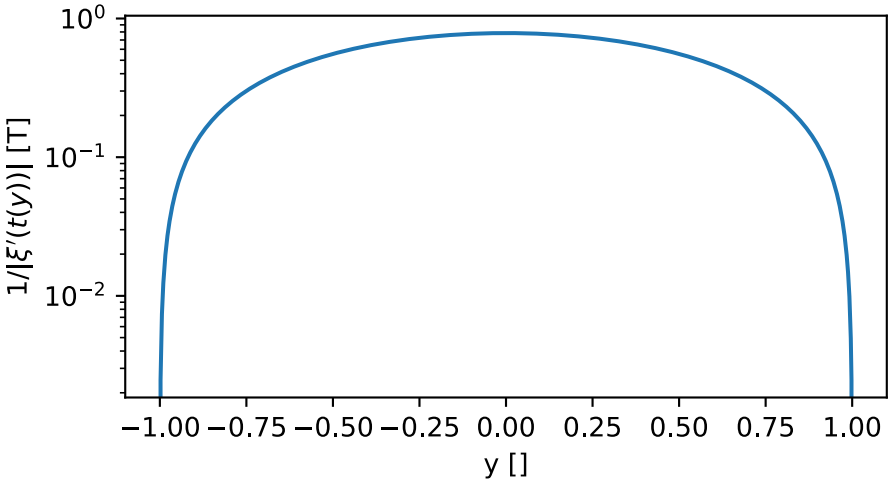

Figure 19: *Plot of the inverse of the derivative of the modulation function in units of the modulation period T against the function value of the modulation function. With the transformations to reach amplitude against frequency this is the shape that describes the dependence of the amplitude on the frequency of the VCO output signal*

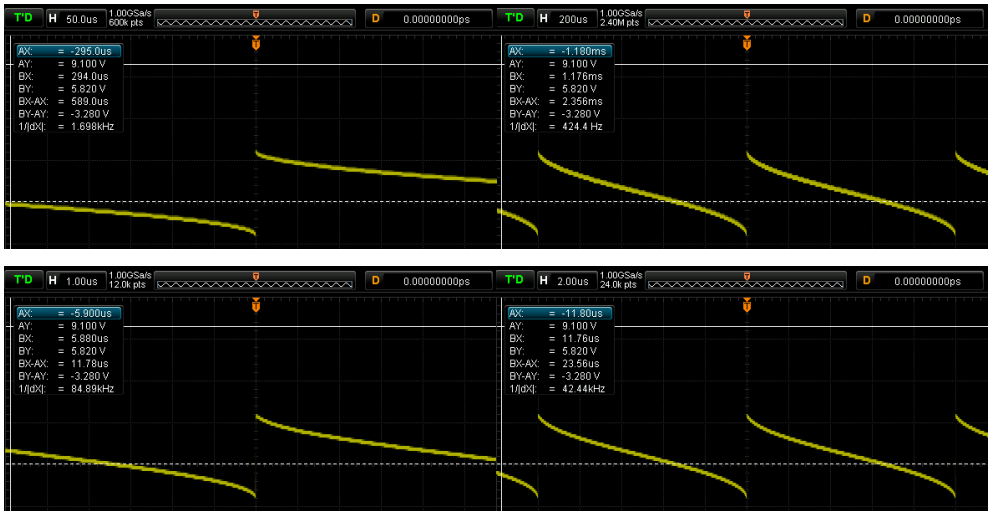

Figure 20: *Pictures of the waveform generated by the function generator at modulation frequencies* **top:** $f_{\text{mod}} = 1\,\text{kHz}$ **bottom:** $f_{\text{mod}} = 100\,\text{kHz}$. *Each are shown in a closer view and a more distant view.*

4.2 Optical Set-up

4.2.1 Optical set-up after AOD

The goal of the optical set-up is to generate the aforementioned time averaged potential for better loading of the atoms. To achieve this one needs to build an array of lenses after the AOD that fulfill three conditions:

1. Manipulate the laser beam such that it is focused at the position of the atoms.
2. Give the beam the wanted waist.
3. Manipulate the direction of the modulated beam in such a way that the beams corresponding to different driving frequencies at the AOD are parallel after the last lens.

The first two conditions are the basic requirements for a regular ODT. The condition that is now new for modulated potentials is that the beams deflected to different angles should be parallel after the lenses. This is required because otherwise the modulation will have a different amplitude at different positions.
Without practical limitations fulfilling all conditions can be achieved with a single lens with the correct focal length. It is then positioned directly in the middle of the AOD and the wanted trap position with the distance to both being the focal length. As in the actual experiment there are limitations on the incoming beam waist as well as the distance of the last lens to the trapped atoms one needs a telescope to achieve the wanted beam waist. Therefore one now has three lenses that are used to manipulate the beam, with some restrictions on their placement.

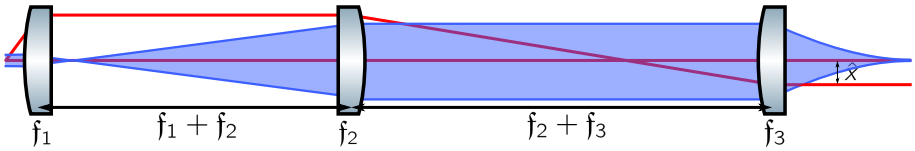

Figure 21: *Lens set-up after the AOD. The lenses are indexed in the order the light passes through them and the distances between the different lenses and their foci are to scale. The red lines trace the path of the center beam as well as a modulated beam. The blue beam shows the effect of the lenses on a Gaussian beam. The different colors are not on the same scale.*

In the set-up after the AOD (figure 21) only focusing lenses are used with two neighbouring lenses always set-up as a telescope, i.e. the distance between them equals the sum of their focal lengths f_i. The AOD is then placed the focal length of the nearest lens away (on the left in figure 21) and the same happens on the side of the atoms (on the right in figure 21). This ensures that, regardless of what lenses are finally chosen, collimated light from the AOD will be focused at the position of the atoms whereas the beams diffracted into different angles by the AOD will have a fixed distance from each other after the last lens. To now chose the correct focal lengths one has to take into consideration what practical limitations are given.
In our case this is the beam waist at the AOD of ca. $w_0 = 550\,\mu m$ as well as a minimum distance to the atoms of 25 cm. Further the beam waist at the position of the atoms is

supposed to be $w_3 \in [20, 30]\mu m$. Additional to these conditions that would also apply for a regular trap with fixed geometry, one has to consider how large the modulation amplitude $\hat{x}$ should be after the last lens. This requirement arises due to the aspect ratio (AR) of the potential, which is the ratio of the width of the trap in modulation direction x and the perpendicular direction z, one would like to be possible to achieve with the tunable geometry. To change the modulation amplitude $\hat{x}$ one can change the frequency range in which the signal for the AOD is modulated. There are limits to this of course as the AOD has a limited bandwidth as discussed in section 3.3.
Considering the constraints provided one can calculate the beam waist w_2 that is needed in front of the last lens to produce $w_3 \in [20, 30]\mu m$ given that the last lens has a focal length of $f_3 = 250\,mm$. This means by using

$$w_3 = \frac{\lambda f_3}{\pi w_2} \Leftrightarrow w_2 = \frac{\lambda f_3}{\pi w_3} \tag{49}$$

one ends up with a required beam waist of $w_2 \in [2.8, 4.2]mm$ after the first two lenses. This then makes the magnification of the telescope made up of the first two lenses to be in the range $M = \frac{f_2}{f_1} \in [5.1, 7.6]$. In general the relation between w_3 and w_0 is then given by

$$w_3 = \frac{\lambda}{\pi w_0} \frac{f_3 f_1}{f_2} \tag{50}$$

In this experiment a 60 mm and a 500 mm focal length lens are used (see figure 22) which theoretically results in $M = 8.\overline{3}$ and $w_3 = 18.5\,\mu m$. In practice this does not produce the theoretical waist but a slightly larger value so that we achieve the beam waist goal set before.

Now that we know that the set-up could work as a regular optical dipole trap as it fulfills the first two conditions stated in the beginning of this section it is time to investigate the modulation of the potential. Therefore one needs to calculate the modulation amplitude $\hat{x}$ after the lens system. For this one needs to assure oneself first that the diffracted beams are indeed parallel at the position of the atoms. In the described case that is shown in figure 21 this is the case if the AOD is placed at the focal point of the first lens, i.e. at the left edge of the figure. We will assume that the AOD deflects the beam at an angle β with respect to the center beam. This then means the deflected beam has a distance

$$d_1 = \sin(\beta) f_1 \tag{51}$$

with respect to the center beam at the position of the first lens. After the first lens the beams are parallel such that they will be parallel again after the next two lenses as those work as an telescope with magnification $M = \frac{f_3}{f_2}$. Thus this leads to the following equation for the modulation amplitude

$$\hat{x} = \sin(\beta) \frac{f_3 f_1}{f_2} \tag{52}$$

Due to the fact that for a change of the AR only the relative size q of waist to modulation amplitude is important a change of the focal lengths does actually not help to modify this as

$$q = \frac{w_x}{\hat{x}} = \frac{\lambda}{\pi \sin(\beta) w_i} \tag{53}$$

Therefore with a set-up of three lenses it is found that the only way to decrease q is to maximise the beam waist of the beam sent through the AOD and to maximise the range of

deflection angles so that $\sin(\beta)$ gets as large as possible. To maximise $\sin(\beta)$ one uses the Bragg condition (42) for the first order ($m = 1$). Assuming small angles we get that

$$\beta = |\theta - \theta_{\text{center}}| \approx |\sin(\theta) - \sin(\theta_{\text{center}})| = \frac{\lambda}{v_s}\Delta f \tag{54}$$

with v_s the sound speed of the AOD crystal and $\Delta f = |f - f_{\text{center}}|$ the difference in sound frequency, which means $q \propto \frac{1}{\Delta f}$. The limitation on Δf and its effect for the modulation amplitude were already mentioned in the previous section (see 4.1.1).

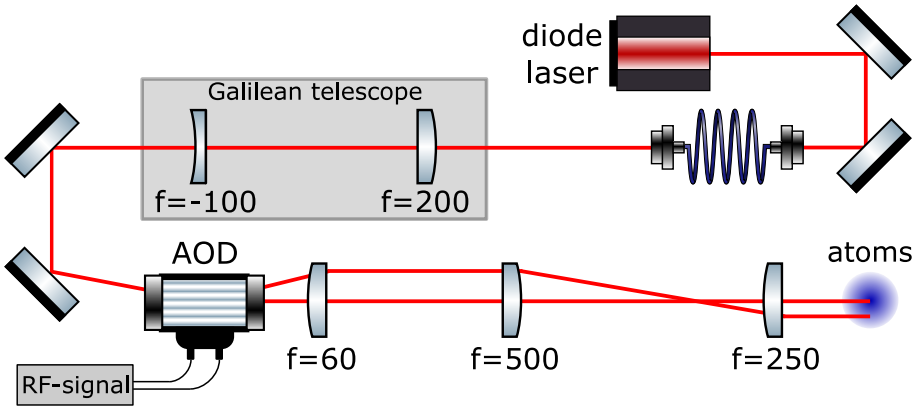

Figure 22: *Sketch of the optical set-up. Only the distances between the last three lenses with respect to each other and to the atoms are to scale. The focal lengths are given in millimeters. As in this thesis there was no actual trapping performed the 'atoms' are there to show the idea of the set-up. In this thesis this position is occupied by a camera.*

4.2.2 Optical set-up before the AOD and beam shaping

In practice one of course has to first acquire the light going through the AOD. For this preparatory work a diode laser was used which had to be coupled into a fiber to ensure a good Gaussian mode of the beam. After the fiber outcoupler the beam waist is roughly two times as large as needed for the AOD which is corrected via a telescope. The set-up for this can be seen in figure 22. When implemented in the actual experiment the laser that will be used is already coupled into a fiber.

One has to check if the set-up works as intended and one hindrance there is for example astigmatism, which would mean that the foci of the beam in the two directions perpendicular to the propagation direction are not at the same position. This is checked here by measuring the beam waist at different positions after the last lens, i.e. around the position of the atoms in figure 22. The beam waist was measured using a beam profiler[13] whose pixel size is $5.5\,\mu\text{m} \times 5.5\,\mu\text{m}$. Due to spacial restrictions two additional mirrors were used between lenses 2 and 3 of figure 21. This leads to the data points shown in figure 23.
To the beam waists that are acquired this way then a fit for the beam waist at the focus as well as the position of the focus via (9) is performed with the additional parameter M^2, the

[13] Dataray CMOS beam profiler WinCamD-LCM

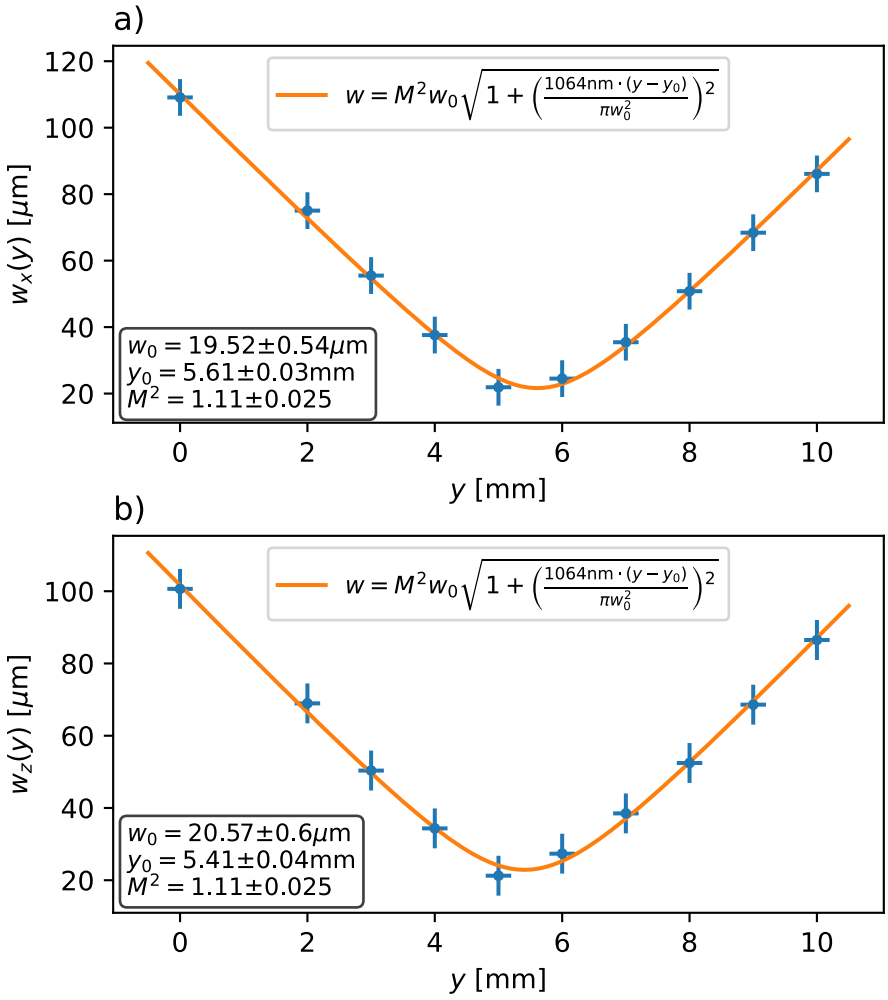

Figure 23: *Plots used to check for astigmatism as well as beam waists in the two directions perpendicular to the propagation direction.* **a)** *beam waist in modulation direction* **b)** *beam waist perpendicular to modulation direction.*

so-called figure of merit to account for an non-perfect Gaussian beam. The results of this are also displayed in figure 23.
To quantify the astigmatism one has to compare the distance between the foci $y_{0,x} - y_{0,z} = 0.20(5)\,\text{mm}$ to the Rayleigh length of the beam $z_{R,x} \approx 1.1\,\text{mm}$. As the astigmatism $y_{0,x} - y_{0,z}$ remains small compared to the Rayleigh length $z_{R,x}$ here one can ignore the slight deviations it induces in the potential that the atoms see.
Furthermore the fit yields an estimate for the beam waists $w_{3,x}$, $w_{3,z}$ at the foci positions. To note here is that one has to be careful as the minimal waist is in this case not given by $w_{\text{fit},i}$ alone but by $M^2 w_{\text{fit},i}$ which then results in the values $w_{3,x} = 21.7(8)\,\mu\text{m}$ and $w_{3,z} = 22.8(8)\,\mu\text{m}$. Thus we can see here that the goal of a waist of 20 µm to 30 µm is achieved. It is also clear that the beam before modulation is not perfectly round, but as the deviation is not extremely large this is not a problem.

5 Experiment - Result

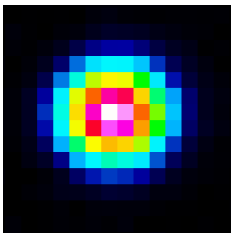

Figure 24: *Picture of the normalised intensity of the unmodulated beam. Pixel size:* 5.5 μm $\times$ 5.5 μm

In this chapter the focus will be on the time averaged potentials that can be achieved using the presented set-up. For this the effects of the modulation frequency and amplitude will be visualised by capturing images where the exposure time is multiple times the period of the modulation. For this again the Dataray beam profiler is used.

The unmodulated beam, i.e. the beam that is used to generate the time averaged potentials, can be seen in figure 24 whose waists were determined to be $w_x = 20.6\,\mu m$ and $w_z = 22.8\,\mu m$ in this position. These values have an error due to the size of the pixels which is ca. 10 %. As the camera was not moved until the last series of pictures, when checking the shape along the propagation direction, this remains the basis for calculations (as later seen in figure 26)

In the following paragraph the standard values for the parameters concerning the modulation are given. These will be used throughout the whole chapter unless it is specified otherwise. Due to the issues present at the modulation frequency of 25 kHz (which would usually be used) a modulation frequency of 1 kHz will be the standard. The issue occurring at 25 MHz can be seen in figure 25 and was described in section 4.1.2. The offset of the tuning voltage of 6 V is kept the same for all measurements and pictures as it corresponds to the deflection of the beam which was used to set up the optical elements. The reason for this choice is that an offset of 6 V corresponds to the center frequency of the AOD that was found in section 4.1.1. The standard for the modulation amplitude of the tuning voltage will be ± 2 V. The maximal possible value, where the tuning voltage is modulated by ± 4 V, was avoided as this was seen to enhance the issue with the frequency output of the VCO.

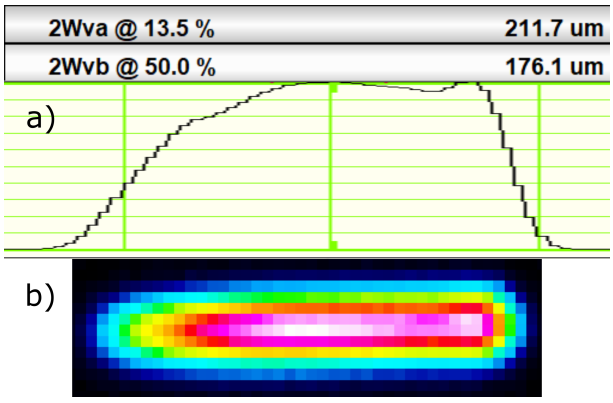

Figure 25: *Modulation with* ± 4 V *and arccosine at a modulation frequency of* 25 kHz. **a)** *Plot of the intensity along the modulation direction with the additional peak observed in the frequency spectrum (figure 18.a)). The distances given are the diameters at* 13.5% $\approx \exp(-2)$ *and* 50% *of the maximal intensity.* **b)** *Picture of the normalised intensity.*

First we will compare different modulation functions and the time averaged potential they produce with the predicted shape. After this there will be three further measurement series to investigate the effects of modulation frequency and amplitude as well as the position along the propagation axis in more detail.

5.1 Comparison of different modulation functions

In the following the captured pictures of the time averaged intensity of the 4 modulation functions arccosine, sine, ramp and square-wave will be compared to the theoretical calculation of the corresponding potential. The modulation functions as well as the corresponding potentials are depicted in figure 26. To note is that the modulation functions are depicted in such a way that they fulfill the conditions set in section 3.1 for the modulation function $\xi(t)$. In the case of the square-wave and the arccosine the implementation of the functions is to just repeat the functions as shown in figure 26 but for the other two functions, namely sine and ramp, the shown function is first followed by its negative such that the implementations at the function generator of both functions are continuous.

The calculations for the modulation with an arccosine were shown before (see 3.1.1) and for the other 3 modulation functions shown in figure 26 they can be found in the Appendix (see B.1). The results as well as the captured pictures are normalised but use different color scales. The beam waists w_x and w_z that were assumed for the calculation were taken from the picture of the unmodulated beam shown in figure 24 with the help of the Dataray software. The modulation amplitude $\hat{x} = 66\,\mu\text{m}$, i.e. $q \approx 0.31$, was determined via the square-wave-modulation with the help of the Dataray software. This will be covered in more detail in section 5.2.
Starting with the picture of the square-wave-modulation shown on the right in figure 26.a) we can see that the potential is split into two parts that both have a very similar shape to the unmodulated potential. Due to imperfections in the set-up and the limited resolution of the camera the two spots are not actually exactly equal. In the theoretical case shown by the plot on the left they are exactly equal which is also clear from the fact that the modulation function $\xi(t)$ is 1 or -1 for the exact same time.
The next potential we will look at is the time averaged potential created by the modulation with an arccosine which is depicted in figure 26.b). One can see that its general shape looks very similar to the original Gaussian potential but stretched along the modulation direction. Here there is some slight asymmetry perpendicular to the propagation axis but it is hard to say how strongly it actually deviates due to the pixel size of the camera. As it otherwise does look quite similar to the calculated potential shown to its left, one can say that it is overall quite similar to the prediction although there are some notable differences.
For the two remaining modulation functions (c: sine and d: ramp) it is possible to see some asymmetry along the modulation in the pictures taken. As there seems to be less intensity in both of the respective bottom right corners this has to be a systematic error. Whether this is a result of a less sensitive camera area or due to an optical element is difficult to determine accurately and thus would need more time and possibly equipment. Therefore this falls out of the scope of this thesis and is not pursued further.

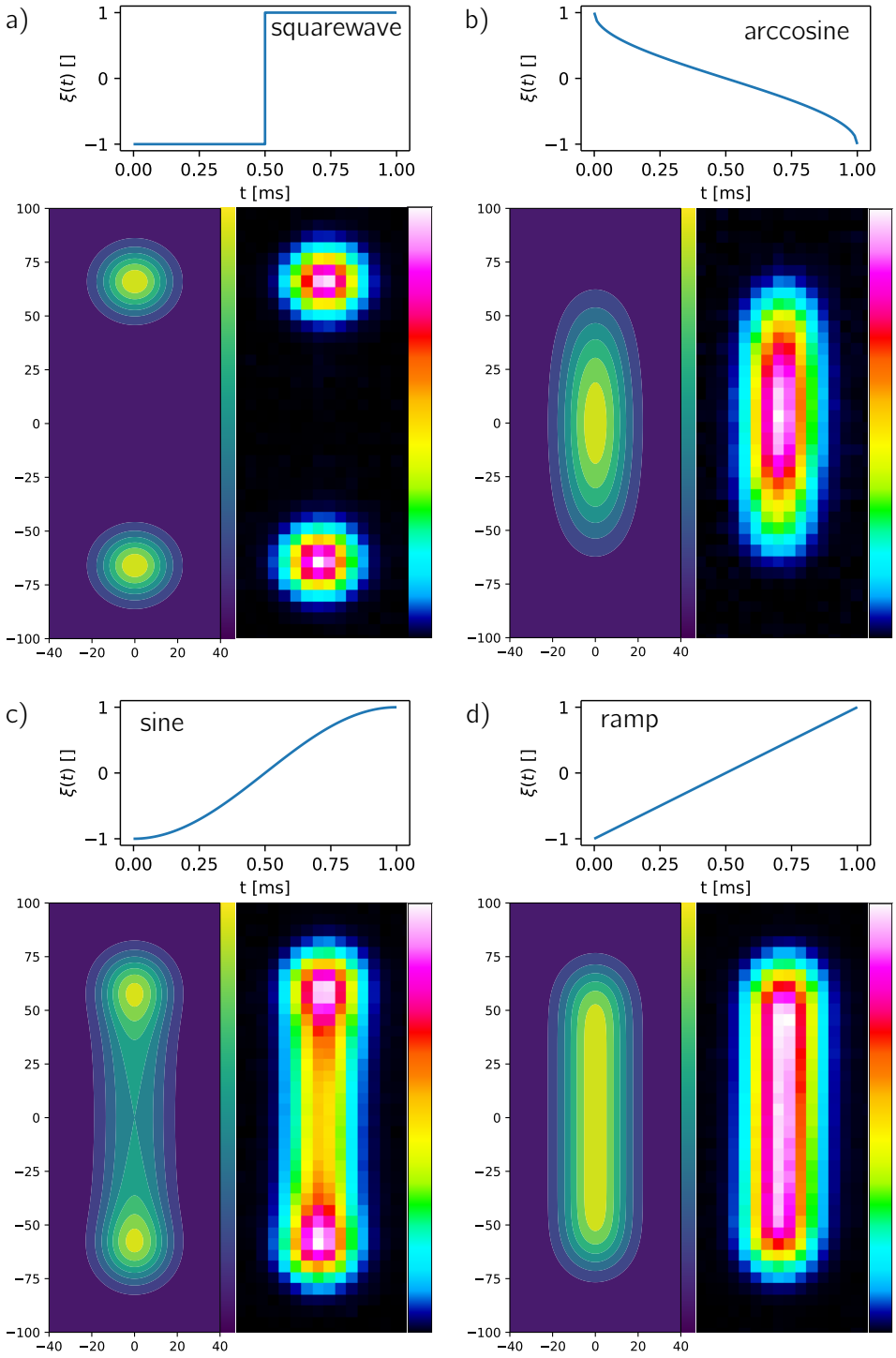

Figure 26: *Plots and pictures of the time averaged intensity of the laser beam for different modulation functions. The parameters of the beam and modulation in the calculation are* $w_x = 20.6\,\mu\text{m}$, $w_z = 22.8\,\mu\text{m}$ *and* $\hat{x} = 66\,\mu\text{m}$. *The modulation function is always depicted above the two images of which the calculated plot is to the left and the picture taken with the camera on the right. Note that the intensities are normalised and plot and picture are displayed with different color scales as shown to the right of the respective image.*

After comparing the pictures to their prediction another point one can make is that, within limits, not only are the generated potentials similar to the prediction but also the modulation amplitude determined via the square-wave-modulation works very well for the other modulation functions. Hence one can be sure that none of the modulation functions tested here (for a small modulation frequency) have no noticeable effect on the modulation amplitude.

5.2 Influence of the modulation frequency

Now that it is clear that the modulation seems to work as intended in the first test with the different modulation functions, we start to look at the effects of the modulation frequency on the potential. The measurement that is done is similar to the one done in figure 17, where the frequency range of the VCO was examined, with the difference that now the modulation amplitude $\hat{x}$ itself will be examined by taking pictures of the beam that is modulated with a square-wave. Determining the distance between the two spots generated by this allows to infer the modulation amplitude as it given as half of this distance. The distance is determined with the help of the Dataray software which determines the positions of the two spots such that one can easily calculate the difference.
The pictures are taken for values of the modulation frequency in the range 1 kHz to 100 kHz. It turns out that there is no discernible change in modulation amplitude until the modulation frequency reaches values above 50 kHz as one can see in figure 27. As such high modulation frequencies are not used anyways this does not pose a problem.
Further one can see that for higher modulation frequencies the amount of light scattered into the region between the two points is increased substantially. This is the result of the VCO with a bandwidth of 100 kHz is nearing its limits at these modulation frequencies and therefore also the intermediate frequencies are taking up a relevant part of the power. In the region that the VCO will be used in practice the effect is not yet extremely strong which means it is not a problem. Another point that further reduces the importance of this effect is the fact that for the modulation with an arccosine, which will mainly be used, there is only one jump per period of the signal and thus the effect is halved. If this would still be unsatisfying one could program a custom function in the function generator by chaining an arccosine and its negative and thus eliminate the jump in frequency entirely. For the other functions which will be shown, namely sine and ramp, there are no jumps to consider anyways as they are continuous and periodic in nature or are programmed without any jumps.

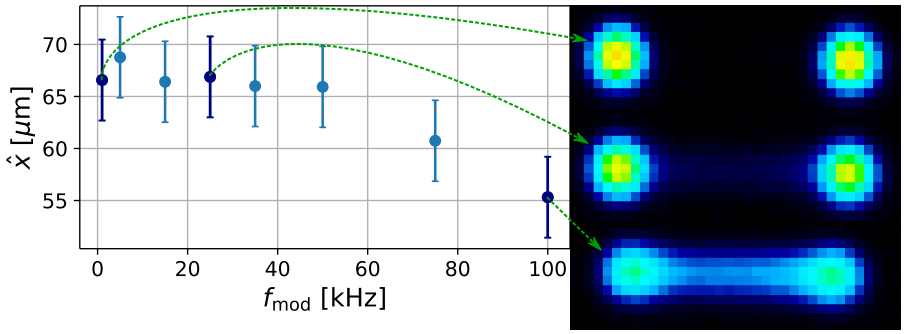

Figure 27: *The plot shows the change of the modulation amplitude with the modulation frequency for a modulation with a square-wave and the three pictures on the right correspond to the marked measurements which are* 1 kHz, 25 kHz *and* 100 kHz.

To sum up the modulation frequency does have adverse effects on the modulation amplitude but only for large modulation frequencies that are not going to be used. Further any function having jumps in its definition will have part of the power scattered roughly evenly over the range of modulation due to the limitations of the VCO. This effect is stronger for higher modulation frequencies and depends on the modulation function that is used.
Therefore the conclusion is that with the correct preparation, i.e. correct function and limited modulation frequency, the modulation frequency does indeed not have a relevant effect on the generated time averaged potential, as calculated before (see chapter 3).

5.3 Influence of the modulation amplitude - Aspect ratio

The second measurement investigates the effect of the modulation amplitude on the shape of the potential with the main focus on the aspect ratio that is achieved. It would be the goal to have the ability to reach an aspect ratio of AR ≥ 10. This means the ratio of modulation amplitude to beam waist has to be of roughly the same size.
For this the modulation is performed with an arccosine varying the modulation amplitude of the tuning voltage given by the function generator in the range $\pm 0.5\,\mathrm{V}$ to $\pm 4\,\mathrm{V}$.

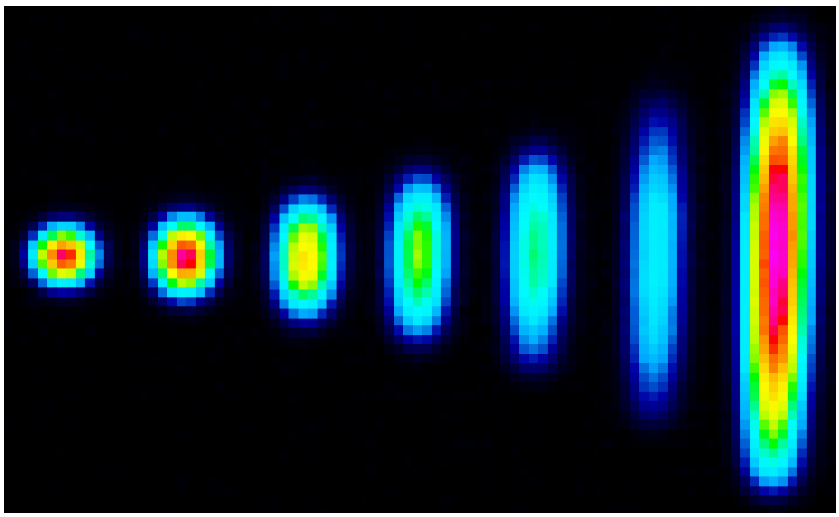

Figure 28: *Pictures of the averaged intensity of the (left to right) unmodulated potential, for modulation with an arccosine and* $V_{\mathrm{mod}} = 0.5\,\mathrm{V},\ 1\,\mathrm{V},\ 1.5\,\mathrm{V},\ 2\,\mathrm{V},\ 3\,\mathrm{V},\ 4\,\mathrm{V}$. *All pictures but the unmodulated potential and the time averaged potential with maximal modulation amplitude have the same exposure time.*

Assuming the presented set-up and constant diffraction efficiency over the whole modulation range (which was also assumed for the calculations of course) for this one would need $\Delta f \approx 24\,\mathrm{MHz}$. Hence the modulation would need to be performed over a range of 48 MHz which is a lot larger than the guaranteed 3 dB bandwidth of the AOD of 32 MHz and even larger than the stated goal 3 dB bandwidth of 40 MHz. This then means that in practice the diffraction efficiency of the AOD will drop noticeably as the range is even larger than the one depicted in figure 16. Therefore the aspect ratio will be significantly smaller than one would expect from the calculation with the assumption of constant diffraction efficiency. Due to the declining diffraction efficiency it is not feasible to achieve large aspect ratios solely by

increasing the used frequency range as this will also change the shape of the potential and will lose a lot of power by diffraction into different orders (especially into the 0th order).
Apart from that the Electronic circuit for the driving frequency used in this experiment does not allow access to the region above $f = 86\,\mathrm{MHz}$ (see section 4.1), which means one would need to use a different function generator or transform the voltage range of the AFG before applying it on the VCO.

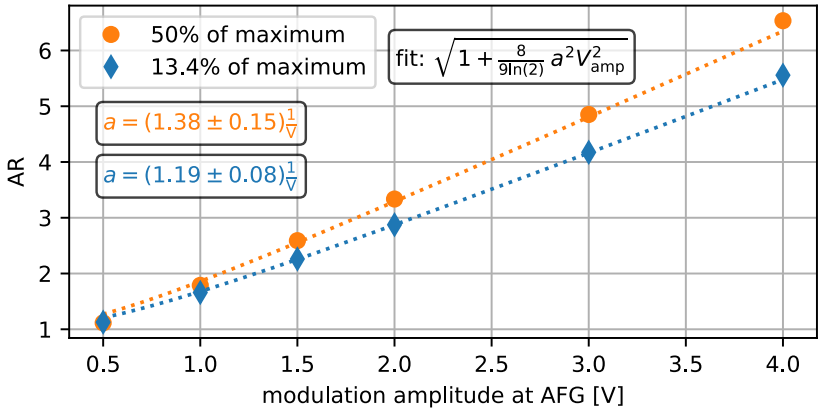

Figure 29: *Plot of the aspect ratio in dependence on the amplitude of the tuning voltage modulation. The values for the AR gained from the diameter at different percentages of the maximum are displayed to show that there is a difference from a perfect Gaussian potential for larger modulation. A fit was performed to compare to the predicted shape. For the error it was assumed that the values for the diameter by the Dataray software have errors given by the pixel size.*

We now investigate the aspect ratio achieved for different amplitudes of the AFG-signal at different depths. Specifically the FWHM and the diameter at $13.4\,\% \approx \exp(-2)$ of the trap depth are chosen to determine the aspect ratio. These values are then determined with the Dataray software.
One finds that the aspect ratio rises with the amplitude as seen in figure 29. This increase is in fact not linear but can be described with the simple model (see (36)) by dividing with the FWHM of the Gaussian beam potential (see (34)), which leads to the formula in figure 29:

$$\mathrm{AR}_{\mathrm{FWHM}} = \sqrt{1 + \frac{8}{9\ln(2)}\frac{1}{q^2}} \qquad \text{with} \qquad \frac{1}{q^2} = a^2 V_{\mathrm{amp}}^2 \tag{55}$$

As this calculation is based on numerical results for the FWHM in modulation direction this formula is originally only useful for the aspect ratio from the FWHM. But as the aspect ratio has always the limit of 1 for low modulation amplitudes and it is reasonable to assume that the trap width at 13.4 % of the trap depth is proportional to the modulation amplitude $\hat{x}$ as well, potentially with a different proportionality constant, one can also use (55) here. The ratios of the fit parameters a will then equal the ratio of these proportionality constants.
To check if the formula gives sensible results we can compare the value for q at $V_{\mathrm{amp}} = 2\,\mathrm{V}$ to the one determined before in section 5.2 where it was $q \approx 0.31$. From the fit for the $\mathrm{AR}_{\mathrm{FWHM}}$ in figure 29 we get $q = \frac{1}{2a\mathrm{V}} = 0.36(4)$. As it is not entirely clear how exact the calculation of parameters is with the Dataray software the error on this value was estimated by assuming the determination of the position to have an uncertainty given by the pixel size

of the camera. This shows that although the values are not equal they are in good agreement such that we can infer that the range for q in this case is given by $q \in [0.18, 1.45]$.
Further we can see that there is a difference in the values determined for the AR at different percentages of the maximum that also increases with the amplitude. The trend visible in the plot can be well understood by reminding oneself of the shape of the time averaged potential for large modulation amplitudes $\hat{x}$ that was discussed before in section 3.2.1. Especially in figure 8 one can clearly see that the FWHM compared to the diameter at 13.4 % is much larger for the modulated potential than it is for the Gaussian beam potential. Due to the fact that the direction perpendicular to the modulation direction does not experience this change and stays Gaussian in shape the values determined for the aspect ratio will diverge further with higher modulation amplitude.
One can also see here that the largest aspect ratio reached in this measurement and thus with this set-up is around 6 (depending on what percentage of the maximal intensity one looks at), which is still quite a bit away from the goal of the aspect ratio being 10 or more.

5.4 Shape along the propagation direction

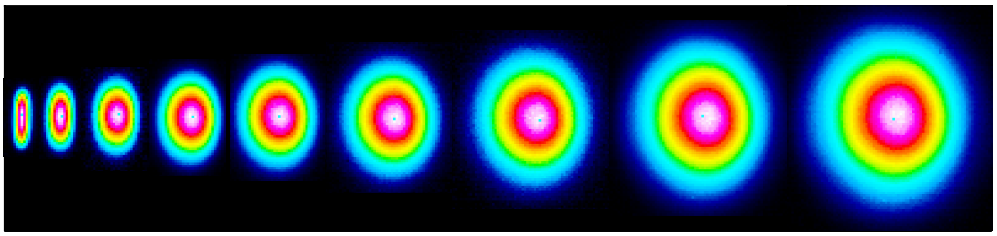

Figure 30: *Pictures taken at different positions along the propagation axis of the laser beam. Every picture was taken at a position* 1 mm *away from the position of the picture(s) next to it.*

The last test that is done with the set-up is to check the shape along the propagation direction. For this the camera is moved away from the focus along the propagation direction (against the beam propagation, i.e. towards the lenses) repeatedly by 1 mm to capture the time averaged intensity at different positions. To note here is that the Rayleigh length of the beam is only slightly larger than 1 mm which means the pictures here were taken over a range of more than seven Rayleigh lengths. The resulting pictures can be seen in figure 30, where one can observe the area that is illuminated grow with the distance as one expects from a focused beam.
For the larger pictures one can see that the averaged intensity is not perfectly symmetric along the direction perpendicular to the modulation direction, that is left to right in the picture, as the maximum in intensity seems to be off-center. As the picture closest to the focus does not have the necessary resolution it is not clear if this is also the case there, but due to the fact that all of the larger pictures seem to possess this characteristic it is sensible to assume that it is. The reason for the maximum being off-center could be one of the optical elements or a tilt of the camera. Such a tilt in the direction in question is quite unlikely and can not be adjusted as it is the direction aligned with the gravitational axis and the beam was made sure to be parallel to the surface.
Regardless of the imperfections the averaged intensity starts from the shape shown in figure 26.b) and then slowly converges to the shape of the unmodulated potential which was shown

close to the focus in figure 24. For a large distance away from the focus the shape should eventually be indistinguishable from the original beam as the modulation becomes irrelevant.

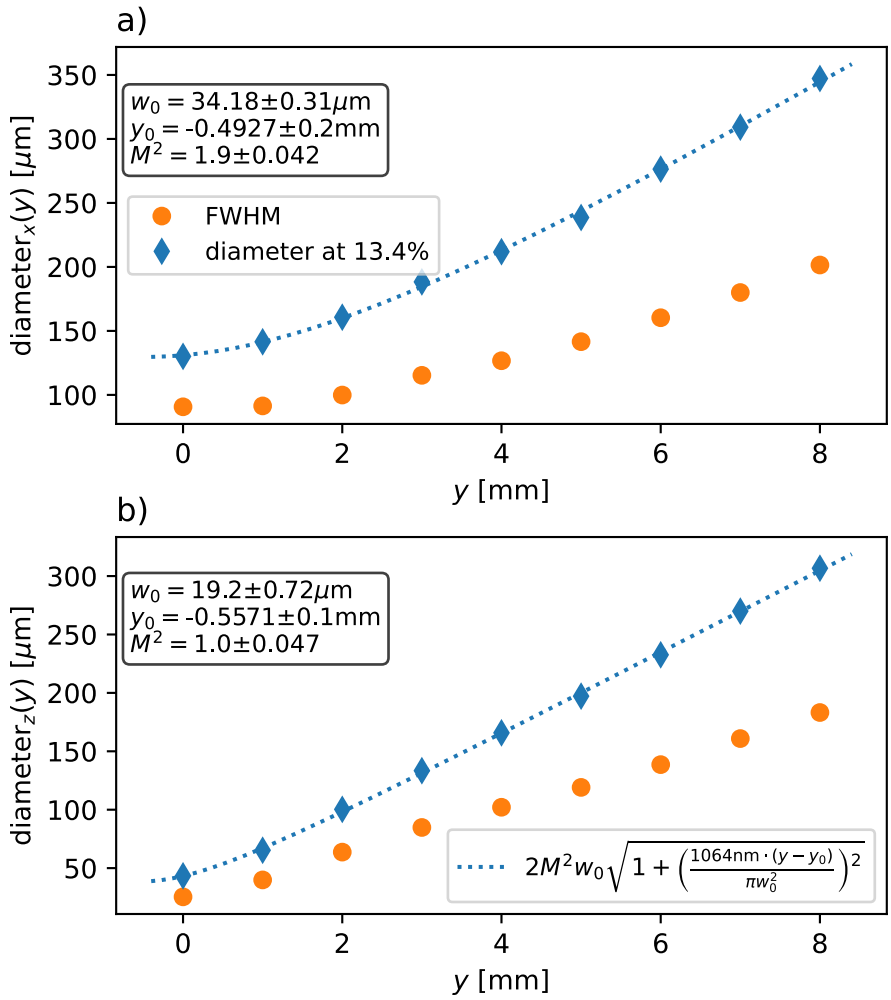

Figure 31: *Plots of the diameter of the trap in modulation direction (x) as well as the direction perpendicular to it (z) at different depths compared to the trap depth. The fit performed is to determine the position of the focus as well as getting an estimate on the trap width at the focus in the approximation of a Gaussian beam potential.*

In figure 31 the diameters in both directions are displayed for the same two levels (50 % and 13.4 %) as before. Here additionally a fit as it was done analogue to the one in figure 23 to get an estimate of the minimal trap diameter in the approximation of a Gaussian beam. The results from this as well as the fit-function are displayed in figure 31.
One can see the diameter of the trap growing at both levels the further one gets away from the focus like one expects. Additionally one can see the gap between the FWHM and the diameter at 13.4 % growing. Comparing the two directions one can easily see that closer to the focus the trap is significantly wider in the modulation direction than it is in the perpendicular direction due to the modulation. For the larger distances one can see that the relative difference in size is not as large anymore.

From the fit results one can also again see that the modulation has a significant effect on the potential shape as the beam in modulation direction has a figure-of-merit of almost 2 whereas the trap in the perpendicular direction can be fitted with an ideal figure-of-merit of 1. One can also reaffirm that there is no relevant astigmatism as the difference between the positions of the foci is not even 10 % of the Rayleigh length.

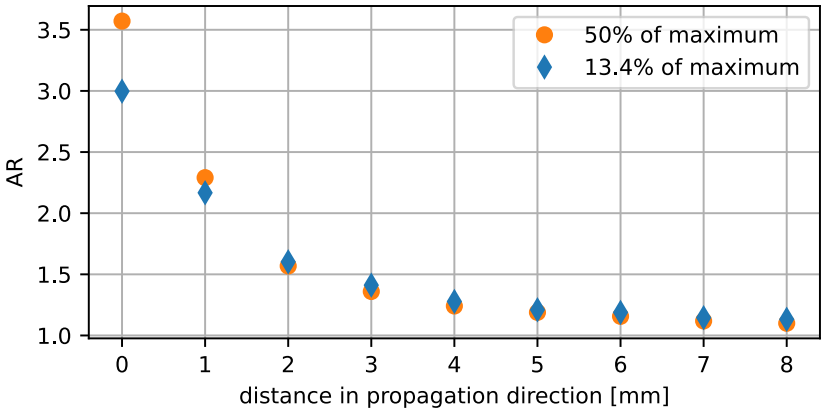

Figure 32: *Plot of the aspect ratio in dependence on the position along the propagation axis. The values for the AR gained from the diameter at different percentages of the maximum are displayed.*

In figure 32 the aspect ratio at the different positions is plotted. One can see that the AR drops the further one moves away from the focus which corresponds to the previously described behaviour. This is also what one would expect to happen as the modulation amplitude $\hat{x}$ remains constant whereas the beam widens when moving away from the focus in propagation direction such that the modulation is less noticeable as it get smaller compared to the beam size. Thus one can say that for large distances from the focus, compared to the Rayleigh length of the original beam, there are no discernible differences between the modulated and unmodulated potential.

6 Conclusion

6.1 Summary

In this thesis a potential set-up for a tunable optical dipole trap was presented. For this we first looked at the theory of optical trapping before using it to determine what to generally expect when periodically moving the beam to modulate the potential the atoms experience. This was then calculated for the case of the modulation with an arccossine as this provides a time averaged potential similar to a Gaussian beam potential. After the theoretical part a possible set-up as well as the results it produced were presented.

After the formula for the time averaged potential was derived to better grasp the characteristics of this potential it was first compared to the potential of a Gaussian beam with the same depth, before the trap depth and width of the modulated potential were examined.
The comparison to a Gaussian beam potential made it obvious that there are some significant differences as soon as the modulation amplitude $\hat{x}$ is larger than the beam waist w_x of the laser beam that is used, i.e. for values of $q = \frac{w_x}{\hat{x}} < 1$. Thus it was found that the time averaged potential can only be described by a Gaussian beam potential for large values of q and the assumption of a Gaussian beam potential is more and more inaccurate the larger the modulation gets, i.e. the smaller q gets.
After this the trap depth was looked at relative to the trap depth of the unmodulated potential, which is the potential the static laser beam produces. For large modulation amplitudes $\hat{x}$, i.e. small q, it was found that in this limit the ratio of the trap depths is equal to q (see figure 12) and for large q the ratio is 1 as the modulation loses its significance:

$$\frac{\hat{U}_{\text{mod}}}{\hat{U}} \approx q \quad \forall q \leq 0.1, \qquad \frac{\hat{U}_{\text{mod}}}{\hat{U}} \approx 1 \quad \forall q \geq 5$$

Although the ranges for q are just a rough estimation, this still leaves the intermediate range of $q \approx 1$ which will have to be used in the experiment of the Quantum Fluids group. Here there was not found such a simple estimation as before for the limits and one would need to use the numerical results in this region or spend more time to find a better estimation than $f(q) = 1 - \exp(-q)$.
In the analysis of the time averaged potential finally the trap width was investigated. As indicator of the trap width here the full width at half maximum (FWHM) was chosen. The simplest description of the FWHM along the modulation direction is given by (36)

$$\text{FWHM}_x \approx \sqrt{\frac{16}{9}\hat{x}^2 + 2\ln(2)w_x^2}$$

which also provides sensible limits but fails to accurately describe the region around $q = 1$ similar as in the case of the trap depth. From this one can also easily see the limits of the FWHM which were found to be $\text{FWHM}_x \to \sqrt{2\ln(2)w_x}$ for $q = \frac{w_x}{\hat{x}} \to \infty$ and $\text{FWHM}_x \to \frac{4}{3}\hat{x}$ for $q \to 0$. Along the propagation direction it is more complicated as an additional parameter influences the beam shape and trap size due to the waist of the beam perpendicular to the modulation direction also playing a role. Due to this there was no deeper analysis performed in this thesis and only an example of the shape for different changes was given in figure 14. The direction perpendicular to the two others is not of great interest as it stays Gaussian in shape and can thus be easily calculated via (34)

In the presented set-up for the AOD driving signal an issue where the VCO output was distorted was noticed for the modulation with an arccosine. As it got worse for increasing modulation frequency (see figure 18), it forced a reduction of the modulation frequency for the pictures that were taken. The reason for this distortion was found to be the VCO.

For the lens system after the AOD a set-up made up from three focusing lenses was presented (see figure 21). This proved to be able to produce the wanted potential but turned out to be rather limited in regards to the influence on the aspect ratio due to the conditions placed on it. Therefore the AR is in fact independent of the focal lengths of the lenses that are used with the given set-up. Hence the aspect ratio can mainly be controlled with the range of the frequency modulation in the AOD driving signal, which is not ideal as it is limited in the electronic circuit presented in the thesis. Further also the diffraction efficiency of the AOD will drop significantly at the edges for a large frequency range and thus limit the achievable AR.

Finally the pictures of time averaged intensities produced with the presented set-up are compared to the predictions that were made based on the calculations of the time averaged potential. It was found that the averaged intensities match quite well with the respective predictions but do have small, notable differences (see figure 26). Further the shape of the potential was observed for different modulation amplitudes $\hat{x}$ where a maximal aspect ratio of ca. 6 was reached.

6.2 Outlook

There are two main points that need to be addressed in a future set-up:

1. The issue with the arccosine-modulation.
2. The achievable aspect ratio.

Resolving the issue in the first point is essential for the set-up to be usable as a tunable ODT as otherwise the atoms can either follow the motion of the trap due to the low modulation frequency or one does not get the wanted trap shape. For this one needs to check the electronic circuit with a different VCO. This VCO can be one of the same model so that one can make sure whether it is an issue with the individual VCO used here or if the model itself is just not suitable for this purpose. In any case one will want to also have another VCO model to compare. An option for this could be the VCO used in the set-up of the master thesis of Claudia Politi [Pol17] which is the Mini-Circuits model ZX95-100. Apart from this one could think about whether it might be worth to manually implement a version of the arccosine at the function generator that does not have a large jump. This might be interesting in the case one wants to also test higher modulation frequencies as otherwise it will not have a large effect.
Although the second point is not as crucial to whether or not the set-up can be used as a tunable ODT a limited aspect ratio takes away from the utility a tunable geometry can provide. To reach larger aspect ratios it is not very sensible to just increase the frequency range of the VCO output as the declining diffraction efficiency of the AOD will reduce the gain in the aspect ratio and also change the shape of the potential. Therefore to increase the aspect ratio that can be reached with a set-up it will be more effective to build a new

lens system after the AOD. This new lens system would need to have at least 4 lenses to add another degree of freedom.

References

[Chi+10] Cheng Chin et al. "Feshbach resonances in ultracold gases". In: *Rev. Mod. Phys.* 82 (2 Apr. 2010), pp. 1225–1286. DOI: 10.1103/RevModPhys.82.1225. URL: https://link.aps.org/doi/10.1103/RevModPhys.82.1225.

[GGP02] Stefano Giovanazzi, Axel Görlitz, and Tilman Pfau. "Tuning the Dipolar Interaction in Quantum Gases". In: *Phys. Rev. Lett.* 89 (13 Sept. 2002). DOI: 10.1103/PhysRevLett.89.130401. URL: https://link.aps.org/doi/10.1103/PhysRevLett.89.130401.

[GWO99] Rudolf Grimm, Matthias Weidemüller, and Yurii B. Ovchinnikov. "Optical dipole traps for neutral atoms". In: (1999). DOI: 10.48550/ARXIV.PHYSICS/9902072. URL: https://arxiv.org/abs/physics/9902072.

[Göl21] Christian Amos Gölzhäuser. "Building a new Dy quantum gas experiment". Bachelor thesis. Heidelberg University, 2021.

[Sch22] Joschka Schöner. "Magnetic-Field Setup for Magneto-Optical-Trapping and Interaction-Tuning in Novel Dysprosium Quantum Gas Experiment". Master thesis. Heidelberg University, 2022.

[ATS05] P. Ahmadi, B. P. Timmons, and G. S. Summy. "Geometrical effects in the loading of an optical atom trap". In: *Phys. Rev. A* 72 (Aug. 2005). DOI: 10.1103/PhysRevA.72.023411. URL: https://link.aps.org/doi/10.1103/PhysRevA.72.023411.

[Lae+03] John R. de Laeter et al. In: *Pure and Applied Chemistry* 75.6 (2003), pp. 683–800. DOI: doi:10.1351/pac200375060683. URL: https://doi.org/10.1351/pac200375060683.

[Poi19] Bureau International des Poids et Mesures. "9th Edition, English version". In: *The International System of Units (SI)* (2019). URL: https://www.bipm.org/en/publications/si-brochure/.

[Mai15] Thomas Maier. "Interactions in a Quantum Gas of Dysprosium Atoms". Dissertation. University Stuttgart, 2015.

[Rav+18] C. Ravensbergen et al. "Accurate Determination of the Dynamical Polarizability of Dysprosium". In: *Phys. Rev. Lett.* 120 (May 2018). DOI: 10.1103/PhysRevLett.120.223001. URL: https://link.aps.org/doi/10.1103/PhysRevLett.120.223001.

[Li+16] H. Li et al. "Optical trapping of ultracold dysprosium atoms: transition probabilities, dynamic dipole polarizabilities and van der Waals C_6 coefficients". In: *Journal of Physics B: Atomic, Molecular and Optical Physics* 50.1 (Dec. 2016). DOI: 10.1088/1361-6455/50/1/014005. URL: https://doi.org/10.1088/1361-6455/50/1/014005.

[Ilz20] Philipp Ilzhöfer. "Creation of Dipolar Quantum Mixtures of Erbium and Dysprosium". Dissertation. University of Innsbruck, 2020.

[LWD14] M. Lepers, J.-F. Wyart, and O. Dulieu. "Anisotropic optical trapping of ultracold erbium atoms". In: *Phys. Rev. A* 89 (2 Feb. 2014). DOI: 10.1103/PhysRevA.89.022505. URL: https://link.aps.org/doi/10.1103/PhysRevA.89.022505.

[Lu14] Mingwu Lu. “Quantum Bose and Fermi Gases of Dysprosium: Production and Initial Study”. Dissertation. Stanford University, 2014.

[Wen15] Matthias Wenzel. “A dysprosium quantum gas in highly controllable optical traps”. Master thesis. University Stuttgart, 2015.

[Bai12] Simon Baier. “An optical dipole trap for Erbium with tunable geometry”. Master thesis. University of Innsbruck, 2012.

[Pol17] Claudia Politi. “Optical dipole trap for an erbium and dysprosium mixture”. Master thesis. University of Innsbruck, 2017.

[McC07] D.J. McCarron. “A Guide to Acousto-Optic Modulators”. In: (2007).

[ST91] Bahaa E. A. Saleh and Malvin Carl Teich. *Fundamentals of Photonics*. 1991.

A Appendix - Optical Trapping

A.1 Gaussian beam

Laser beams are usually described by Gaussian beams, that means they have a characteristic intensity distribution which is given by a two-dimensional Gaussian in the plane perpendicular to the propagation direction. For a Gaussian beam its size varies along the propagation direction due to diffraction.

The waist of a Gaussian beam is defined here[14] as the distance from the intensity maximum at which the intensity is only $\frac{1}{e^2} \approx 13.5\,\%$ of said maximum. The change of this the waist along the propagation direction (in this case chosen to be y) is given by [ST91, p.83]

$$w(y) = w_0 \sqrt{1 + \frac{y^2}{z_R^2}} \tag{56}$$

where w_0 is the waist at the focus. z_R is the Rayleigh length, which is the distance from the focus where the waist is larger by a factor of $\sqrt{2}$. It is given by [ST91, p.83]

$$z_R = \frac{\pi w_0^2}{\lambda} \tag{57}$$

with λ being the wavelength of the laser. Given these definitions one can write the intensity of an elliptical[15] Gaussian beam as [Pol17, p.23][ST91, p.85 (round case)]

$$I(x,y,z) = \frac{2P}{\pi w_x(y) w_z(y)} \exp\left(-2\left(\frac{x^2}{w_x^2(y)} + \frac{z^2}{w_z^2(y)}\right)\right) \tag{58}$$

The effect of focusing lenses on a Gaussian beam is characterised via their waists at the focus, the wavelength of the laser and the focal length f of the lens used [ST91, p.95]

$$w_0' = \frac{w_0}{\sqrt{1 + \left(\frac{z_R}{f}\right)^2}} \overset{z_R >> f}{\approx} w_0 \frac{f}{z_0} \overset{(57)}{=} \frac{\lambda f}{\pi w_0} \tag{59}$$

In the case of telescopes their magnification determines the ratio of the waists before and after the telescope.

A.2 Force of Gaussian beam potential

With the potential for a single Gaussian beam (7):

$$F = -\nabla U = -\begin{pmatrix} \partial_x U \\ \partial_y U \\ \partial_z U \end{pmatrix} \tag{60}$$

$$-\partial_x U = x \frac{4}{w_x^2(y)} U \begin{cases} > 0 & \forall x < 0 \\ = 0 & \text{if } x = 0 \\ < 0 & \forall x > 0 \end{cases} \tag{61}$$

[14] There may be different conventions as $\frac{1}{e^2}$ is an arbitrarily chosen value, albeit it is used often.

[15] The elliptical case is not much harder to handle, but is more general than the round case. Using cartesian coordinates further allows for simpler combination of crossed beams (see 2.3)

$$-\partial_z U = z\frac{4}{w_z^2(y)}U\begin{cases}>0 & \forall z<0\\ =0 & \text{if } z=0\\ <0 & \forall z>0\end{cases} \tag{62}$$

$$-\partial_y U = -y\left[4\left(\frac{x^2}{w_x}\frac{1}{z_{R_x}^2}\left(1+\frac{y^2}{z_{R_x}^2}\right)^{-2}+\frac{z^2}{w_z}\frac{1}{z_{R_z}^2}\left(1+\frac{y^2}{z_{R_z}^2}\right)^{-2}\right) - \frac{\frac{1}{z_{R_x}^2}+\frac{1}{z_{R_z}^2}+2y^2\frac{1}{z_{R_x}^2 z_{R_z}^2}}{1+y^2\left(\frac{1}{z_{R_x}^2}+\frac{1}{z_{R_z}^2}\right)+y^4\frac{1}{z_{R_x}^2 z_{R_z}^2}}\right]\cdot U \tag{63}$$

Therefore for example on the y-axis ($x = z = 0$) we have

$$-\partial_y U = y\cdot\frac{\frac{1}{z_{R_x}^2}+\frac{1}{z_{R_z}^2}+2y^2\frac{1}{z_{R_x}^2 z_{R_z}^2}}{1+y^2\left(\frac{1}{z_{R_x}^2}+\frac{1}{z_{R_z}^2}\right)+y^4\frac{1}{z_{R_x}^2 z_{R_z}^2}}\cdot U\begin{cases}>0 & \forall y<0\\ =0 & \text{if } y=0\\ <0 & \forall y>0\end{cases} \tag{64}$$

A.3 Influence of tensor polarisability

Assuming one uses linearly polarised light of a fixed wavelength, $\tilde{\alpha}$ can be written in the form

$$\tilde{\alpha}(\theta_p) = \Re(\alpha_s) + \frac{3M_J^2 - J(J+1)}{J(2J-1)}\cdot\frac{3\cos^2(\theta_p)-1}{2}\Re(\alpha_t) \tag{65}$$

as ω is fixed and the second term drops out due to $\mathcal{A} = 0$.
The value of $\tilde{\alpha}$ then only depends on the state of the respective atom and the angle θ_p between laser polarisation and magnetic field axis. α_s and α_t are the same for all atoms.
θ_p will be approximately the same for all atoms in the trap so it will not introduce differences between the different atoms. This holds strictly for plane waves of light, but in the case of real applications one has to use waves with imperfect wavefronts. As the wavevector stands perpendicular to the wavefront its direction changes according to the wavefront errors when moving out of the center of the beam. Due to the fact that the polarisation of light is always transversal and thus perpendicular to the wavevector, the angle θ_p might change for different positions. As it will turn out the uncertainties to θ_p do not matter much for the trap depth, but it's individual effect on atoms at different positions will have an effect on the optical potential even though it will be small.
This leaves the state of the atoms as a possible difference between individual atoms. As this experiment produces spin-polarised gases with $M_J = -J$ this is also an effect that will apply to all atoms equally.

Now that it is determined that the created optical potential will be approximately the same for all atoms in the trap, one can look at the possible range of values for $\tilde{\alpha}$. With the spin-polarisation of the atoms range of possible values is independent of the value of J. We had (65) with the scalar and tensor parts of the polarisability being fixed for a given wavelength of the laser. Now we have the variables $M_J = -J$ and $\theta_p \in [0, \pi] \subset \mathbb{R}$ which means:

$$3\cos^2(\theta_p) - 1 \in [-1, 2] \tag{66}$$

$$\Rightarrow 3M_J^2 - J(J+1) = 2J^2 - J \tag{67}$$

$$\Rightarrow \frac{3M_J^2 - J(J+1)}{J(2J-1)} = \frac{2J^2 - J}{J(2J-1)} = 1 \tag{68}$$

$$\Rightarrow \frac{3M_J^2 - J(J+1)}{J(2J-1)} \cdot \frac{3\cos^2(\theta_p) - 1}{2} \in [-0.5, 1] \tag{69}$$

$$\Rightarrow \tilde{\alpha} \in [\Re(\alpha_s) - 0.5\Re(\alpha_t),\ \Re(\alpha_s) + \Re(\alpha_t)] \tag{70}$$

$$\Rightarrow \Delta\tilde{\alpha} = 1.5\Re(\alpha_t) \tag{71}$$

This remaining uncertainty of the value is given due to the arbitrary orientation of the laser polarisation into the trap. The real part of the tensor part of the polarisability is smaller than the corresponding value of the scalar part by two orders of magnitude for the chosen wavelength of 1064 nm [Rav+18][Li+16]. Hence it is possible to disregard the dependence on θ_p of $\tilde{\alpha}$ for the case of this thesis as it will not greatly affect the depth of the potential.

A.4 Additional plots

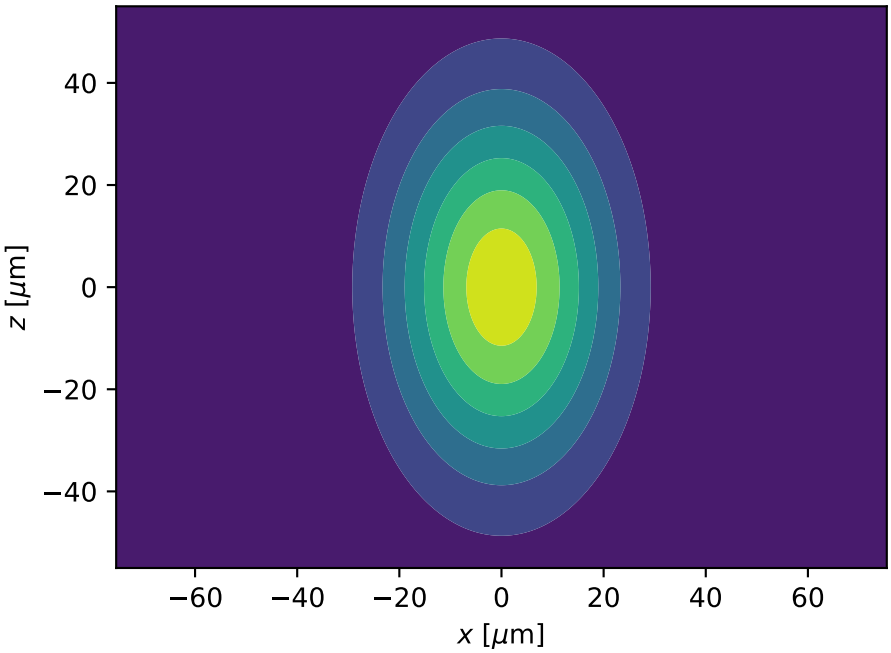

Figure 33: *This figure is the contour-plot counterpart to figure 1*

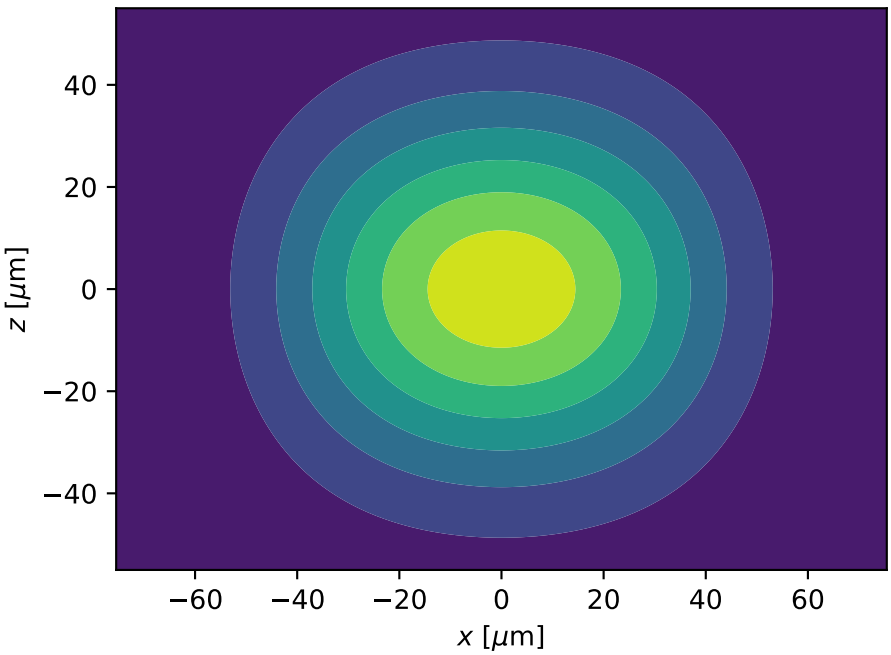

Figure 34: *This figure is the contour-plot counterpart to figure 3*

B Appendix - Modulation

B.1 Modulation functions

B.1.1 Linear modulation

For a linear modulation one possible modulation function is

$$\xi(t) = \frac{2t}{T} - 1 \tag{72}$$

The other possibility satisfying the set conditions would be the negative of this, which would give the same results.

$$\xi'(t) = \frac{2}{T} \tag{73}$$

$$\Rightarrow \frac{1}{\xi'(\xi^{-1}(\tilde{x}-\mu))} = \frac{T}{2} \tag{74}$$

$$U_{\text{mod}}(x,y,z) = -\frac{P\mathfrak{c}}{\pi w_x(y) w_z(y)} \exp\left(-2\frac{z^2}{w_z^2(y)}\right) \cdot \int_{\tilde{x}-1}^{\tilde{x}+1} \exp\left(-2\frac{\mu^2}{q^2(y)}\right) \mathrm{d}\mu \tag{75}$$

$$U_{\text{mod}}(x,y,z) = -\frac{P\mathfrak{c}\exp\left(-2\frac{z^2}{w_z^2(y)}\right)}{\pi w_x(y) w_z(y)} \cdot \frac{q(y)}{2}\sqrt{\frac{\pi}{2}}\left[\text{erf}\left(\sqrt{2}\frac{\tilde{x}+1}{q(y)}\right) - \text{erf}\left(\sqrt{2}\frac{\tilde{x}-1}{q(y)}\right)\right] \tag{76}$$

B.1.2 Discret modulation

The integral can be replaced with a sum for discret levels $n \in \mathcal{N} \subset [-1,1]$. This leads to the following potential:

$$U_{\text{mod}}(x,y,z) = -\frac{2P\mathfrak{c}\exp\left(-2\frac{z^2}{w_z^2(y)}\right)}{\pi w_x(y) w_z(y)} \cdot \sum_{n\in\mathcal{N}} a_n \exp\left(-2\frac{(\tilde{x}-n)^2}{q^2(y)}\right) \tag{77}$$

with $\sum_{n\in\mathcal{N}} a_n = 1$. For the case of a regular square-wave this leads to

$$U_{\text{mod}}(x,y,z) = -\frac{P\mathfrak{c}\exp\left(-2\frac{z^2}{w_z^2(y)}\right)}{\pi w_x(y) w_z(y)}\left[\exp\left(-2\frac{(\tilde{x}+1)^2}{q^2(y)}\right) + \exp\left(-2\frac{(\tilde{x}-1)^2}{q^2(y)}\right)\right] \tag{78}$$

B.1.3 Sinusoidal modulation

Using a sine one gets the modulation function

$$\xi(t) = \sin\left(\pi\frac{t}{T} - \frac{\pi}{2}\right) \tag{79}$$

$$\xi'(t) = \frac{\pi}{T}\cos\left(\pi\frac{t}{T} - \frac{\pi}{2}\right) \tag{80}$$

$$\xi^{-1}(\zeta) = T\left(\frac{1}{\pi}\arcsin(\zeta) + \frac{1}{2}\right) \tag{81}$$

$$\Rightarrow \xi'(\xi^{-1}(\zeta)) = \frac{\pi}{T}\cos\left(\arcsin(\zeta)\right) \tag{82}$$

$$= \frac{\pi}{T}\sqrt{1-\zeta^2} \tag{83}$$

$$\Rightarrow \frac{1}{\xi'(\xi^{-1}(\tilde{x}-\mu))} = \frac{T}{\pi}\frac{1}{\sqrt{1-(\tilde{x}-\mu)^2}} \tag{84}$$

Therefore the potential is given by

$$U_{\text{mod}}(x,y,z) = \frac{2P\mathfrak{c}\exp\left(-2\frac{z^2}{w_z^2(y)}\right)}{\pi^2 w_x(y)w_z(y)} \cdot \int_{\tilde{x}-1}^{\tilde{x}+1} \frac{\exp\left(-2\frac{\mu^2}{q^2(y)}\right)}{\sqrt{1-(\tilde{x}-\mu)^2}}\mathrm{d}\mu \tag{85}$$

This does not have a nice solution and has to be integrated numerically. In this case one might rather use the original version (see 21) to compute the integral.

B.2 Additional plots

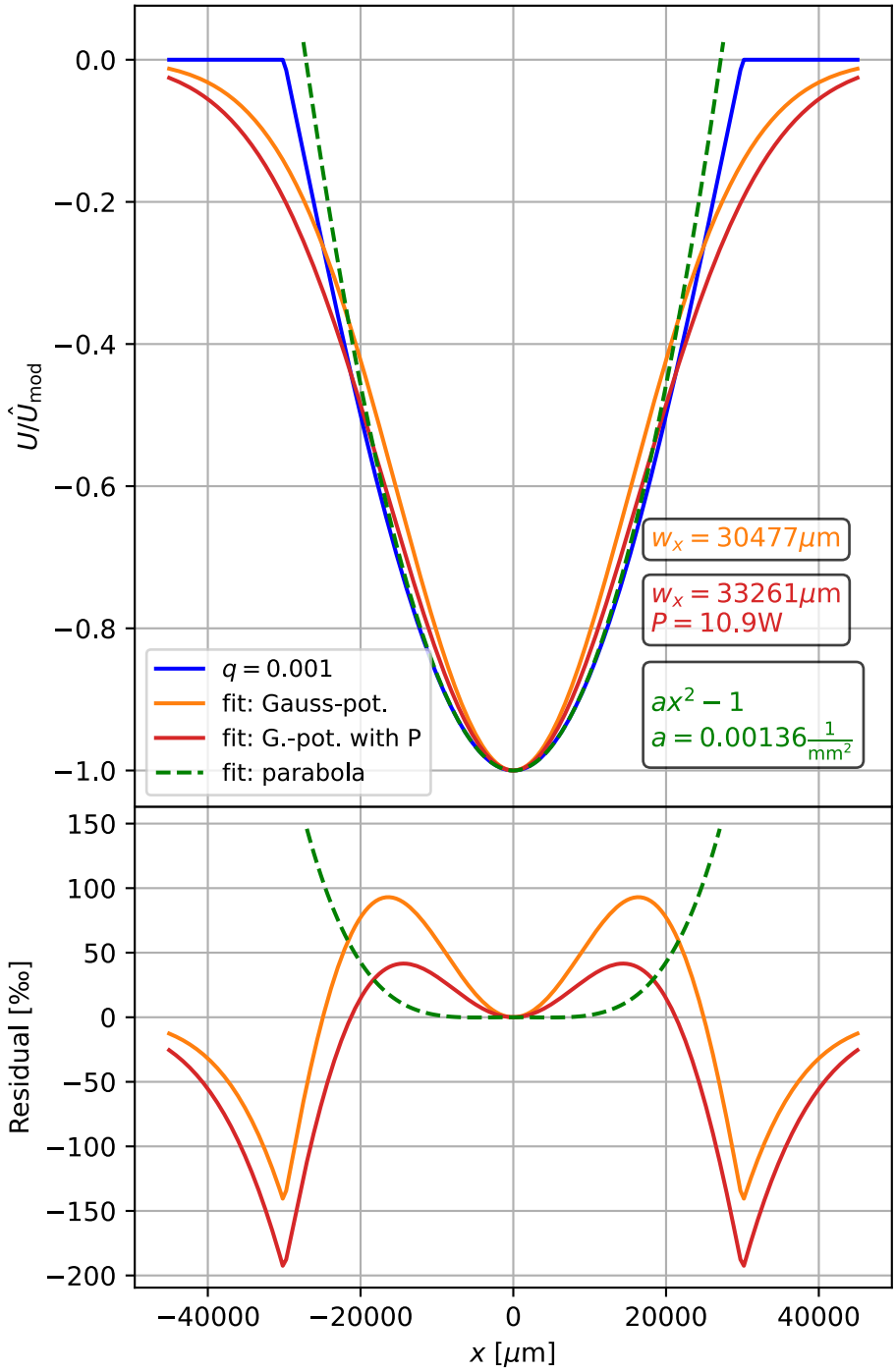

Figure 35: *Comparison of a time-averaged potential with $q = \frac{1}{1000}$ and a fitted Gaussian potential as well as a parabola along the modulation direction ($y = z = 0$). The fit function (7) has all values but w_x (and P) fixed to the same values as the modulated potential. Note that the parabola is just fit to the central region of the potential.* **Top**: *Plot of the potentials normalised to the trap depth of the modulated potential;* **Bottom**: *Plot of the differences between the normalised potentials ($U_{\mathrm{fit}} - U_{\mathrm{mod}}$).*

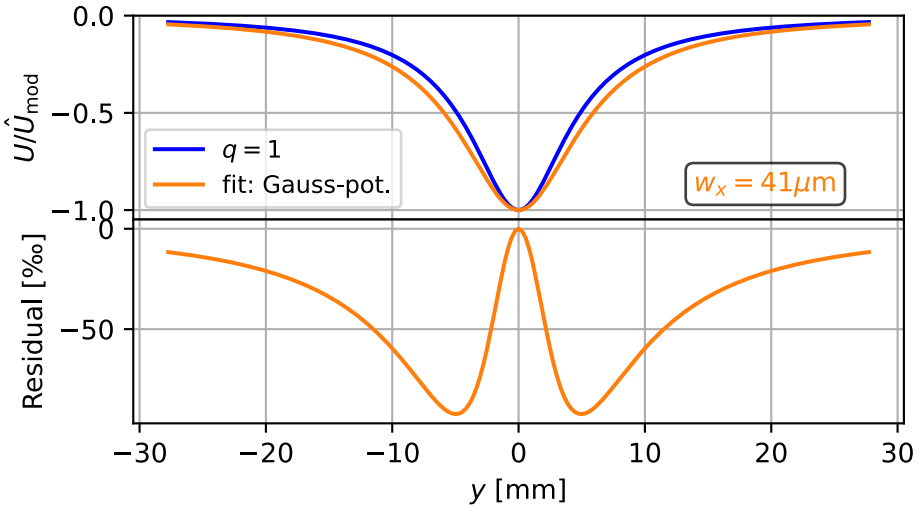

Figure 36: *Comparison of a time-averaged potential with $q = 1$ and a fitted Gaussian potential along the propagation direction ($x = z = 0$). The fit function (7) has all values but w_x fixed to the same values as the modulated potential.* **Top***: Plot of the potentials normalised to the trap depth of the modulated potential;* **Bottom***: Plot of the differences between the normalised potentials ($U_{\mathrm{fit}} - U_{\mathrm{mod}}$).*

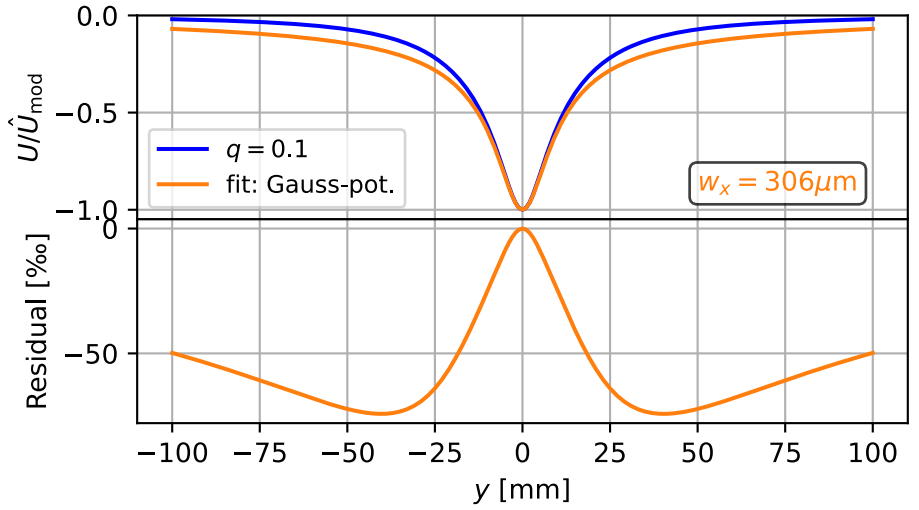

Figure 37: *Comparison of a time-averaged potential with $q = \frac{1}{10}$ and a fitted Gaussian potential along the propagation direction ($x = z = 0$). The fit function (7) has all values but w_x fixed to the same values as the modulated potential.* **Top***: Plot of the potentials normalised to the trap depth of the modulated potential;* **Bottom***: Plot of the differences between the normalised potentials ($U_{\mathrm{fit}} - U_{\mathrm{mod}}$).*

Acknowledgements

I would like to thank the whole Quantum Fluids group for being ready to answer questions or discuss different topics. I want to especially thank my supervisor Prof. Dr. Lauriane Chomaz for being available for questions at any time as well as the discussions about my project and the helpful tips. Similarly I would like to thank Dr. Shuwei Jin for answering my various questions especially regarding the practical work of setting up an optical system.
Further I would like to thank Prof. Dr. Wolfram Pernice for being my second examiner.

Finally I want to thank my parents for always supporting me as well as my friends for making studying so much more fun.

Erklärung

Ich versichere, dass ich diese Arbeit selbstständig verfasst und keine anderen als die angegebenen Quellen und Hilfsmittel benutzt habe.

Heidelberg, den 22.09.2022,

Paul Holzenkamp